



MSU Graduate Theses

Spring 2021


Development of a Laser-Assisted Chemical Vapor Deposition (CVD) Technique to Grow Carbon-Based Materials

Abiodun Ademola Odusanya

Missouri State University, Abiodun234@live.missouristate.edu

As with any intellectual project, the content and views expressed in this thesis may be considered objectionable by some readers. However, this student-scholar's work has been judged to have academic value by the student's thesis committee members trained in the discipline. The content and views expressed in this thesis are those of the student-scholar and are not endorsed by Missouri State University, its Graduate College, or its employees.

Follow this and additional works at: <https://bearworks.missouristate.edu/theses>

 Part of the [Nanoscience and Nanotechnology Commons](#), and the [Semiconductor and Optical Materials Commons](#)

Recommended Citation

Odusanya, Abiodun Ademola, "Development of a Laser-Assisted Chemical Vapor Deposition (CVD) Technique to Grow Carbon-Based Materials" (2021). *MSU Graduate Theses*. 3617.
<https://bearworks.missouristate.edu/theses/3617>

This article or document was made available through BearWorks, the institutional repository of Missouri State University. The work contained in it may be protected by copyright and require permission of the copyright holder for reuse or redistribution.

For more information, please contact bearworks@missouristate.edu.

**DEVELOPMENT OF A LASER-ASSISTED CHEMICAL VAPOR DEPOSITION (CVD)
TECHNIQUE TO GROW CARBON-BASED MATERIALS**

A Master's Thesis

Presented to

The Graduate College of
Missouri State University

In Partial Fulfilment

Of the Requirements for the Degree
Master of Science, Materials Science

By

Abiodun Ademola Odusanya

May 2021

© 2021, Abiodun Ademola Odusanya

DEVELOPMENT OF A LASER-ASSISTED CHEMICAL VAPOR DEPOSITION (CVD) TECHNIQUE TO GROW CARBON-BASED MATERIALS

Physics, Astronomy and Materials Science

Missouri State University, May 2021

Master of Science

Abiodun Ademola Odusanya

ABSTRACT

Carbon-based materials (CBMs) including graphene, carbon nanotubes (CNT), highly ordered pyrolytic graphite (HOPG), and pyrolytic carbon (PyC) have gained so much attention in research in recent years because of their unique electronic, optical, thermal, and mechanical properties. CBMs are relatively very stable and have minimal environmental footprint. Various techniques such as mechanical exfoliation, pulsed laser deposition, and chemical vapor deposition (CVD) have been used to grow CBMs and among them thermal CVD is the most common. This study aims to explore ways of reducing the energy requirement to produce CBMs, and for that, a novel pulsed laser-assisted CVD technique had been developed in our laboratory. The growth pattern was monitored by altering various growth parameters like gas flow rate, temperature, laser energy, and deposition time. CBMs were grown both on Si and Cu substrates, and better quality CBM films were found on Cu as it acts as a catalytic agent for two-dimensional growth. Raman spectroscopy confirms the presence of high quality PyC which was grown with optimum parameters (temperature of 750°C, CH₄ gas flow rate of 20sccm, a laser frequency of 10Hz, energy density of 0.116J/cm² per pulse). It is found that the local pulsed-laser bombardment helps in breaking the carbon-hydrogen bonds of CH₄ at much lower temperature than its thermal decomposition temperature (1000°C-1200°C). With the further increase of temperature there was no significant change in the 2D peak intensity in Raman spectrum which is the indicator of the number of graphene layer. The intertwined graphene flakes of the PyC cause some surface roughness which is responsible for quenching the Raman 2D signal. Further development is needed to achieve a single layer of graphene and other 2D materials using the laser-assisted CVD technique.

KEYWORDS: CVD, CBMs, PyC, Laser, Graphene, 2D materials, Laser-assisted CVD

**DEVELOPMENT OF A LASER-ASSISTED CHEMICAL VAPOR DEPOSITION (CVD)
TECHNIQUE TO GROW CARBON-BASED MATERIALS**

By

Abiodun Ademola Odusanya

A Master's Thesis
Submitted to the Graduate College of
Missouri State University
In Partial Fulfilment of the Requirements
For the Degree of Master of Science, Materials Science

May 2021

Approved:

Kartik Ghosh, Ph.D., Thesis Committee Chair

Ridwan Sakidja, Ph.D., Committee Member

Tiglet Besara, Ph.D., Committee Member

Julie Masterson, Ph.D., Dean of the Graduate College

In the interest of academic freedom and the principle of free speech, approval of this thesis indicates the format is acceptable and meets the academic criteria for the discipline as determined by the faculty that constitute the thesis committee. The content and views expressed in this thesis are those of the student-scholar and are not endorsed by Missouri State University, its Graduate College, or its employees.

ACKNOWLEDGEMENTS

I am immensely grateful to my research advisor, Dr Kartik Ghosh for the persistent help he rendered from the very beginning of my thesis right until the very end, his priceless contributions, suggestions, and provisions will always be remembered. I would like to thank Dr Robert Mayanovic for allowing me to use the Raman spectroscopy machine which was an essential tool for the characterization of my sample.

My sincere thanks to Brian Grindstaff for his efforts in helping me with the designing and machining of essential components for the success of my project and not forgetting Mike Murphy for his tremendous help when I had challenges with some electrical devices. I will not forget to mention the likes of Nick Rogers for the gas line setup and Sinjan Majumder for making himself available during the piping and vacuum testing of the gas lines.

Utmost thanks to my family here in the United States and back home in Nigeria for the enormous moral support they gave me as I faced challenges during my thesis work. I would not have made it this far without them.

TABLE OF CONTENTS

Chapter 1: Introduction	Page 1
1.1 Motivation	Page 1
1.2 Introduction to graphene	Page 1
1.3 Common ways of producing graphene	Page 2
1.4 Properties and applications of graphene	Page 6
1.5 The CVD technique and factors affecting it	Page 7
1.6 Common CVD reactors and mode of operation	Page 12
1.7 Objectives of the thesis	Page 15
Chapter 2: Experimental	Page 16
2.1 Design and engineering	Page 16
2.2 Gas flow assembly	Page 17
2.3 Optical assembly	Page 25
2.4 Heating system	Page 27
2.5 Sample preparation and process flow	Page 29
2.6 Characterization	Page 31
Chapter 3: Results and discussion	Page 34
3.1 Data presentation and analysis	Page 34
3.2 Variation of CH ₄ flow rate and temperature	Page 37
3.3 Variation of time	Page 44
3.4 Effect of laser energy on PyC deposition	Page 48
3.5 Effect of substrate on PyC deposition	Page 49
3.6 Reaction mechanism for PyC deposition	Page 50
3.7 Quantitative analysis of results	Page 52
Chapter 4: Conclusions and future works	Page 55
References	Page 57

LIST OF TABLES

Table 1.1 Comparison of graphene obtained by different methods	Page 5
Table 1.2 Classification of reactors and distinguishing features	Page 14
Table 2.1 MFC gauge Factors	Page 20
Table 3.1 Process parameters for silicon and copper substrate via resistive heating	Page 35
Table 3.2 Constant CH ₄ flow rate at 10sccm and varied temperature	Page 37
Table 3.3 Constant CH ₄ flow rate at 20sccm and varied temperature	Page 41
Table 3.4 Constant CH ₄ flow rate at 20sccm, temperature and varied time	Page 45
Table 3.5 Effect of laser energy on PyC deposition	Page 48
Table 3.6 Ratio of peak intensities and number of layers	Page 53
Table 3.7 Peak positions, intensities, and number of layers	Page 54

LIST OF FIGURES

Figure 1.1 (a) Hexagonal structure of 2D graphene (b) 0D buckminsterfullerene (c) 1D CNT	Page 2
Figure 1.2 Classification of graphene synthesis techniques	Page 5
Figure 1.3 Precursor transport and reaction processes in CVD	Page 8
Figure 1.4 Schematic of growth process model in CVD	Page 12
Figure 1.5 Schematic diagram of the tube reactor	Page 13
Figure 1.6 Schematic diagram of the showerhead reactor	Page 15
Figure 2.1 Custom-built laser-assisted CVD chamber	Page 16
Figure 2.2 Schematic diagram of a mass flow controller (MFC)	Page 18
Figure 2.3 Front panel controls	Page 19
Figure 2.4 Rear panel controls	Page 19
Figure 2.5 Schematic diagram of the roughing/rotary vane pump	Page 23
Figure 2.6 Schematic diagram of the turbomolecular pump	Page 24
Figure 2.7 Schematic diagram of the Nd:YAG laser	Page 26
Figure 2.8 Schematic diagram of the deposition process in the chamber	Page 26
Figure 2.9 Resistive heater and induction furnace	Page 28
Figure 2.10 PID temperature controller	Page 28
Figure 2.11 P&ID chart for laser-assisted CVD via resistive heating	Page 30
Figure 2.12 P&ID chart for laser-assisted CVD via inductive heating	Page 30
Figure 2.13 Molecular vibrations and Raman scattering	Page 33
Figure 2.14 Diagram of the Rayleigh and Raman scattering processes	Page 33
Figures 3.1 (a-c) Raman spectra of pristine silicon, copper, and high-quality graphene	Page 36
Figures 3.2 (a-d) Raman spectra at constant CH ₄ flow rate at 10sccm and varied temperature	Page 38

Figures 3.2 cont'd (e-j) Raman spectra at constant CH ₄ flow rate at 10sccm and varied temperature	Page 39
Figures 3.3 (a-f) Raman spectra at constant CH ₄ flow rate at 20sccm and varied temperature	Page 42
Figures 3.3 cont'd (g-l) Raman spectra at constant CH ₄ flow rate at 20sccm and varied temperature	Page 43
Figures 3.3 cont'd (m-o) Raman spectra at constant CH ₄ flow rate at 20sccm and varied temperature	Page 44
Figures 3.4 (a-b) Raman spectra at constant CH ₄ flow rate of 20sccm, temperature and varied time	Page 45
Figures 3.4 cont'd (c-f) Raman spectra at constant CH ₄ flow rate of 20sccm, temperature and varied time	Page 46
Figures 3.5 (a-c) Raman data plots showing effect of pulsed laser on PyC deposition	Page 48
Figures 3.6 Raman data plots showing effect of pulsed laser on PyC deposition	Page 50
Figure 3.7 Energy profile for the complete dehydrogenation of CH ₄	Page 52

INTRODUCTION

1.1 Motivation

From the beginning of time, scientists have always sought out ways to improve the quality of life and ease of doing things. As we got smarter, the utilization of simple tools and common elements found in our surroundings enabled us to test and push the limit of our capabilities and make both steady and quantum leaps in areas of human welfare, healthcare, utilities, and manufacturing - all these being as a result of newer materials having superior properties than the former.

Considering these, recent research and development has been geared towards producing more efficient and cost-effective materials in the quest of making that special material that minimizes trade-offs between properties needed for its intended use. One of these wonder materials is graphene, -a single layer atomic thick of graphite which possesses excellent electronic mobility, mechanical stiffness, flexibility, and chemical properties¹. Graphene is made through a number of ways one of which include mechanical exfoliation and thermal CVD, but if we desire more control over the growth properties, the latter is preferred. Using thermal CVD, graphene is typically grown between 1000°C and 1050°C²⁻³. Our goal is to deposit graphene on a copper substrate at a much lower temperature using pulsed laser as a secondary source of energy.

1.2 Introduction to graphene

What is graphene? As stated earlier, graphene is one atom thick layer of graphite, its sp² hybridized atoms (meaning the mixing of one s and two p atomic orbitals by promoting one

of the electrons in the s-orbital to one of the 2p orbitals) are held together in a hexagonal honeycomb lattice with each carbon atom tightly bound to its 3 neighboring atoms as shown in the Figure 1.1(a), it can be wrapped into a buckyball (b) or rolled into carbon nanotube (CNT) (c) below. This 2D material is the fundamental building block of all graphitic materials and has a molecular bond length of 0.142 nm with a tensile strength of 130GPa and a Young's modulus of 1TPa. It is a remarkable conductor of heat with conductivity at between $(4.84 \pm 0.44) \times 10^3$ to $(5.30 \pm 0.48) \times 10^3 \text{ W} \cdot \text{m}^{-1} \cdot \text{K}^{-1}$) and $200,000 \text{ cm}^2 \cdot \text{V}^{-1} \cdot \text{s}^{-1}$ respectively⁴.

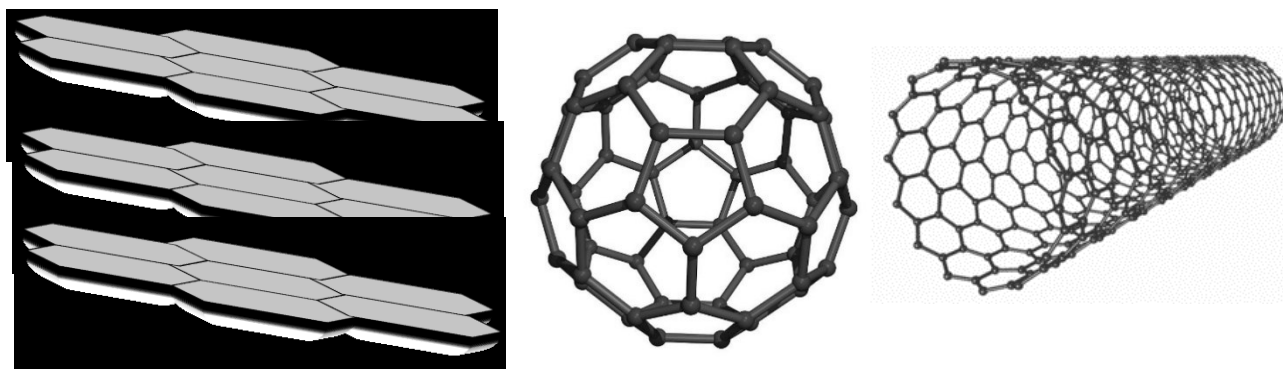


Figure 1.1 (a) Hexagonal structure of 2D graphene (b) 0D buckminsterfullerene (c) 1D CNT

1.3 Common ways of producing graphene

Graphene can be synthesized either physically or by chemical means. In this section, we will address all the available means of producing graphene as at the time of writing this thesis as shown in the Figure 1.2 below.

1.3.1 Mechanical exfoliation: This method remains the most popular and perhaps the most convenient means of making graphene. This is otherwise known as the “scotch tape” method, and it involves placing a scotch tape on a block of graphite, removing it and placing

another scotch tape on the initial one, peeling it off and repeating the process a few times like 20 times to obtain a single layer graphene (SLG) or a few layer graphene (FLG).

1.3.2 Liquid-phase exfoliation: In this technique, chunks of graphite are finely crushed in a graphite mill, and these fine particles of graphite are sucked in through a suction chamber into a pipe leading into an ultrasonication chamber in which they are finely dispersed in a suitable solvent like acetic acid, sulfuric acid and hydrogen peroxide. Inside the sonication chamber, samples collected at the bottom of the chamber have the greatest number of layers of graphene, while those collected at the top have the least. This process is very much synonymous to material processing technique of comminution and concentration. However, this process is not effective for bulk production of high-quality few-layer graphene.

1.3.3 Reduction of graphene oxide (RGO): This process involves the initial oxidation of graphite to graphite oxide (GO) and further reduction to graphene. There are three common techniques used for this process namely: Hummers', Staudenmaier, and Brodie's method⁷. What makes these three different are the reagents used, the reaction temperature, and the reaction time.

For instance, the Hummers' method involves soaking graphite in H_2SO_4 and $KMnO_4$ to obtain GO, and subsequent stirring or sonication results to getting GO in single layers owing to the hydrophilic nature of GO's functional groups. Lastly, chemical, thermal, or electrochemical reduction of the GO are done to obtain graphene albeit this procedure induces high structural defects in graphene⁸.

1.3.4 Epitaxial growth: This technique otherwise known as sublimation method involves the growth of epitaxial graphene (EG) via the thermal decomposition of single-crystal silicon-carbide in ultrahigh vacuum (UHV) and under ambient pressure. The growth process is controlled by the annealing temperature and time. At elevated temperature, the silicon atoms

vaporize, and the carbon-rich layer is left behind and after a series of surface alignment influenced by the annealing temperature and time, graphene of different layer configurations can be formed⁹ possessing different growth rates, morphology, and electronic properties.

The advantage of this is that it can be used for low defect and large surface area fabrication and no subsequent transfer of the graphene is needed which comes very handy in device processing applications¹⁰.

1.3.5 Chemical vapor deposition (CVD): To produce graphene, this method essentially involves use of some precursor gases (one gas or a mixture of gases) to add pressure into the system, and the other to act as a carbon source in a reaction chamber at an elevated temperature in the presence of a suitable substrate. Ar/H₂ gas is often times used to add pressure into the system while CH₄ is used as the carbon source because of its low dehydrogenation energy compared to other hydrocarbons. Using thermal CVD technique, graphene is typically grown between 1000°C and 1050°C²⁻³ in the presence of either a copper or nickel substrate. To have graphene deposited on any substrate part of the key considerations are:

1. The substrates should act as a catalyst for graphene growth by promoting the surface solubility of carbon on it.
2. The mass diffusion and flux from the gas phase and the substrate surface should be sufficient to allow the carbon source gas populate the chamber and the gas needs to diffuse to the reaction zone.

Further details on the CVD technique will be explained in subsequent sections in this chapter.

The Table 1.1 below shows a direct comparison of the type and quality of graphene that can be obtained using various techniques mentioned earlier.

Table 1.1 Comparison of graphene obtained by different methods¹¹.

Method	Sample size	Cost and quality	Different types
Mechanical exfoliation	5-100 μm	High cost, high quality, low yield.	Flakes
Liquid-phase exfoliation	Few nm	High cost, high quality, low yield.	Nano-sheets
Reduction of graphene oxide (RGO)	Few nm	Low cost, low quality.	Nano-flakes
Epitaxial growth on SiC	>50 μm	High cost, high quality, low yield.	Thin films
Chemical vapor deposition (CVD)	$\leq 75\text{cm}$	High cost, high quality.	Thin films

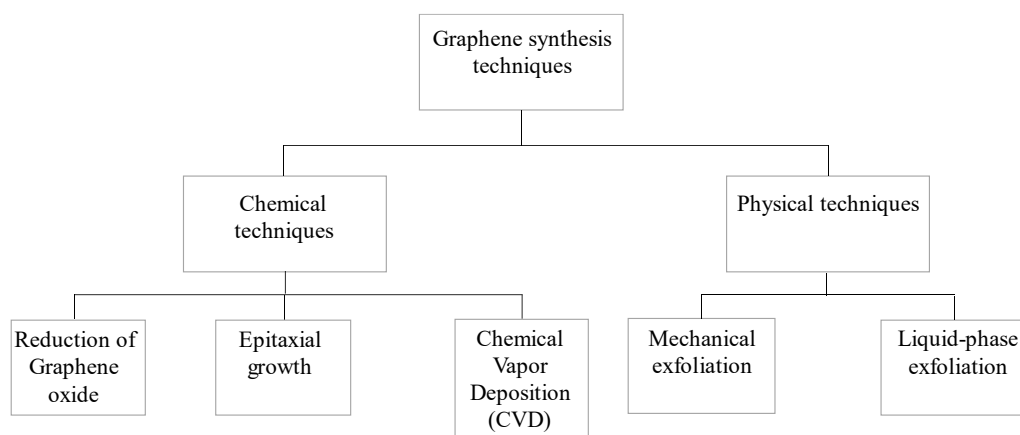


Figure 1.2 Classification of graphene synthesis techniques

1.4 Properties and applications of graphene

1.4.1 Electronic properties: Since the valence band and the conduction band of graphene meet at the Dirac point, graphene is said to have zero bandgap. This is what makes it very high electron mobility because of its zero effective mass near the Dirac point. Very high electron mobility of more than $200,000 \text{ cm}^2\text{V}^{-1}\text{s}^{-1}$ at electron densities of $\sim 2 \times 10^{11} \text{ cm}^{-2}$ has been reported in single layer graphene¹² and this makes it applicable in superconductor applications.

1.4.2 Thermal conductivity: No material surpasses graphene, and it is regarded as the perfect thermal conductor. It has no preferential direction for heat transport (which makes it an isotropic conductor) for in-plane thermal conductivity, and the value recorded for this is between 3000 and 5000 $\text{Wm}^{-1}\text{K}^{-1}$, ten times the value of copper¹³.

1.4.3 Optical properties: As a matter of fact, thinner materials are often more transparent than thicker ones; Graphene being a single layer of sp² hybridized carbon atoms permits more light to pass through than graphite and this can be confirmed by UV-Vis spectroscopy with an atomic layer absorption of 2.3%. This feature is very useful in optoelectronic applications in making transparent conducting electrodes and ultra-fast photodetectors.

1.4.4 Physical / mechanical properties: Defect-free monolayer graphene has intrinsic strength of 130GPa, and this makes it far stronger than steel with a Young's modulus of about 1TPa. In addition, graphene can be stretched to about 25% of its initial length, and this makes it considered a somewhat ductile material. With its high surface area to weight ratio of about 2630m²/g, graphene is lightweight and is impermeable to helium¹⁴. All these make graphene useful in lubricants with anti-wear properties and lightweight structural composites.

1.4.5 Chemical properties: Graphene is a very stable material and can be suitably doped to induce certain characteristics in device applications. In addition, one can add functional groups to graphene, and this makes it have a good potential for drug delivery in pharmaceutical applications. It has been shown that graphene family of nanomaterials (GFNs) have lower toxicity than other carbon nanomaterials, and highly flexible physicochemical properties that allow the various functional groups of the molecule to be altered and perform specific functions¹⁵.

1.5 The CVD technique and factors affecting it

As explained earlier, the CVD technique in simple terms is the use of some precursor gases to have certain reactions in a reaction chamber at elevated temperatures to produce a thin film or a powder on a given substrate. As simple as this sounds, it is important to know that certain factors need to be considered in the CVD technique as far as graphene growth is concerned. These factors include sample preparation, substrate, reactor dimension, reactor temperature, reactor pressure, gas flow rates, sample position, annealing condition, growing condition, and cooling condition¹⁶.

CVD techniques are often conveniently named after the pressure the deposition takes place or the source of energy, and the choice of process influences what the outcome will be:

- Atmospheric pressure CVD (APCVD)
- Low pressure CVD (LPCVD)
- Metal-organic CVD (MOCVD)
- Photon/laser induced CVD (PHCVD)
- Plasma enhanced CVD (PECVD)

- Thermal CVD
- High density plasma CVD (HDPCVD)

All these techniques listed above operate on the same basic principles¹⁷ as seen in Figure 1.3:

1. Evaporation and transport of precursors in the bulk gas flow region into the reactor.
2. Gas phase reactions of precursors in the reaction zone to produce reactive intermediates and gaseous by-products.
3. Mass transport of reactants to the substrate surface.
4. Adsorption of the reactants on the substrate surface.
5. Surface diffusion to growth sites, nucleation and surface chemical reactions leading to film formation.
6. Desorption and mass transport of remaining fragments of the decomposition away from the reaction zone.

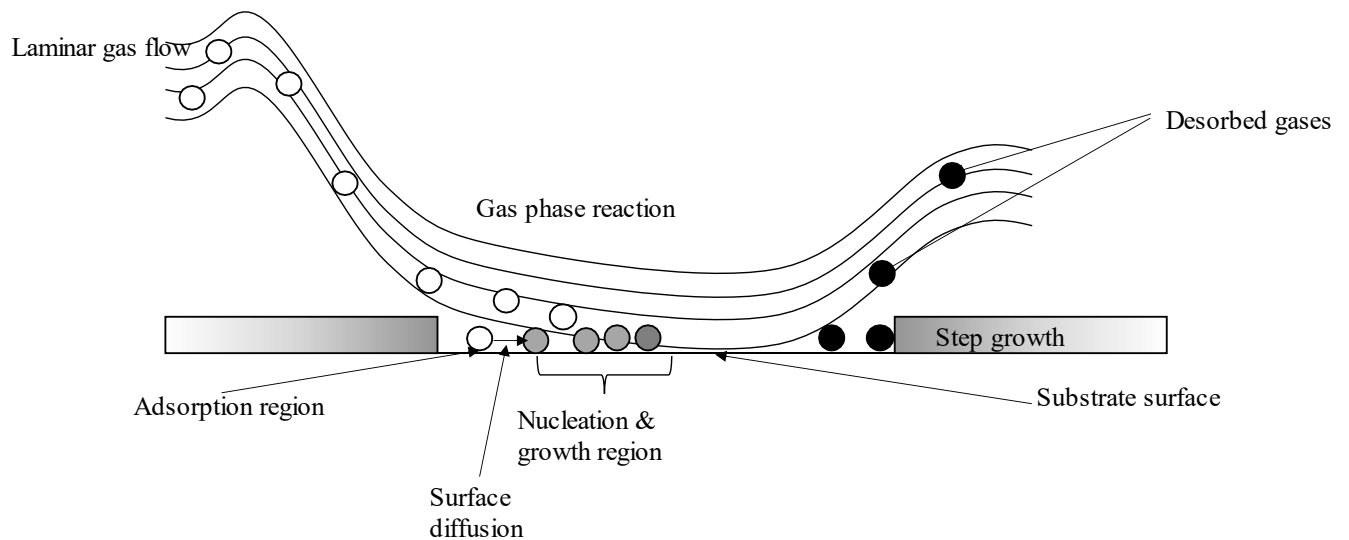


Figure 1.3 Precursor transport and reaction processes in CVD

Understanding the fundamentals of CVD is needed to have a full grasp of what it is, and these are¹⁸:

1. Reaction rates
2. Diffusion
3. Gas transport

Essentially, to have a successful CVD procedure, the precursor gases are made to flow into the reaction chamber by mass transport with the aid of a mass flow controller MFC, and for a typical thermal CVD process, the precursor gases flow through the boundary layer of the heated substrate which marks the reaction region for the process. The precursors and by-products are required to be gaseous, and the reaction process needs to result in a solid deposit in the form of film or powder on the chosen substrate. Depending on the precursor gases used, we can obtain different kinds of reactions in the reaction chamber such as: pyrolysis, reduction, oxidation, compound formation, disproportionation and reversible transfer¹⁸. In CVD processes the nature of gas flow is very essential because this affects the deposition rate and mechanism, and the gas flow needs to be laminar i.e. few hundreds of Reynold's (maximum of a few hundreds) or having the Knudsen number less than one. In agreement with Boundary layer theorem, molecules closest to the boundary have the least velocity during a gas flow process while molecules farthest away have the highest velocity. With this in mind, a stagnant layer is produced right on the substrate-gas interface in the reaction zone, and the molecules remain there just long enough for the appropriate reactions to occur. The thickness of the stagnant layer is often influenced by the conditions in the reactor and the angle the substrate is kept in relation to the incoming gases. At the boundary layer, these parameters are key for deposition to take place¹⁸:

1. Thickness of the stagnant layer δ , $\delta = \frac{10}{3} \frac{L}{\sqrt{Re_L}}$ (1.1)

where L is the distance from the leading edge of the plate

Re is the Reynold's number

2. Diffusion coefficient D, $D = D_o \frac{P_o}{P} \left(\frac{T}{T_o}\right)^n$ (1.2)

where D_o is the diffusion constant at T_o and P_o and n is 1.8

3. Gas flow rate J_i , $J_i = -\frac{D(P_g - P_s)}{\delta RT}$ (1.3)

where P_g is the vapor pressure in bulk gas and P_s is the vapor pressure of the substrate surface

In addition to predicting thermodynamical feasibility of the reaction process, the kinetics of a CVD system needs to be understood to ascertain the rate of the deposition process. The following need to be understood:

- homogeneous reactions taking place among the gases in a reaction chamber
- heterogeneous reactions occurring on the surface of a substrate
- mass transportation of the gaseous precursors.

The overall deposition rate of the CVD process is limited by the slowest step in the three steps mentioned above¹⁹.

Homogeneous chemical reactions take place completely in the gas phase and nucleated products are not incorporated into the crystal structure of the film, whereas heterogeneous reactions occur on a substrate with the nucleated products incorporated into the crystal structure of the film. The kinetics of homogeneous reactions for a CVD process is important to know when ascertaining the gaseous intermediates generated, the amount and chemistry of these species, the stoichiometry of the reaction, and the rate limiting factors.

From Grove's model²⁰, it was concluded that the mass transport of the reactant gaseous species across the boundary layer only depends on the mass diffusion, because of this, there is a

concentration gradient of the gaseous species as seen in Figure 1.4. The flux (J_1) of mass transport from the gas phase of the substrate surface is:

$$J_1 = h_G(C_G - C_S) \quad (1.4)$$

where C_G and C_S are the concentration of reactant gaseous species in the bulk gas phase and at the surface of the substrate, respectively.

$$h_G = \frac{D}{\delta} \quad h_G \text{ is the mass transfer coefficient} \quad (1.5)$$

For first order reactions, the flux (J_2) of the reactant gaseous species consumed on the substrate surface through the heterogeneous reactions is¹⁹:

$$J_2 = k_S C_S \quad (1.6)$$

where k_S is the heterogeneous surface reaction constant.

At steady state, $J_1 = J_2$. Equating equations (1.4) and (1.6), we get:

$$C_S = \frac{C_G}{1 + k_S/h_G} \quad (1.7)$$

For every process that begins, surely there must be an end, at elevated temperatures, these three factors control the rate of reaction: mass transport, surface reactions, and temperature.

If $h_G \gg k_S$, a reaction-limited growth occurs; if $k_S \gg h_G$, a transport-limited growth occurs.

For thermodynamic-limited growth, if the deposition reaction is exothermic, the Gibbs free energy gets less negative with increasing temperature, hence, the growth rate of the coating decreases. But if the deposition reaction is endothermic, the Gibbs free energy is more negative with increasing temperature. Here, the homogeneous reactions are likewise substantially improved, therefore causing a formation of powder in the gas phase as opposed to forming a coat on the substrate¹⁹.

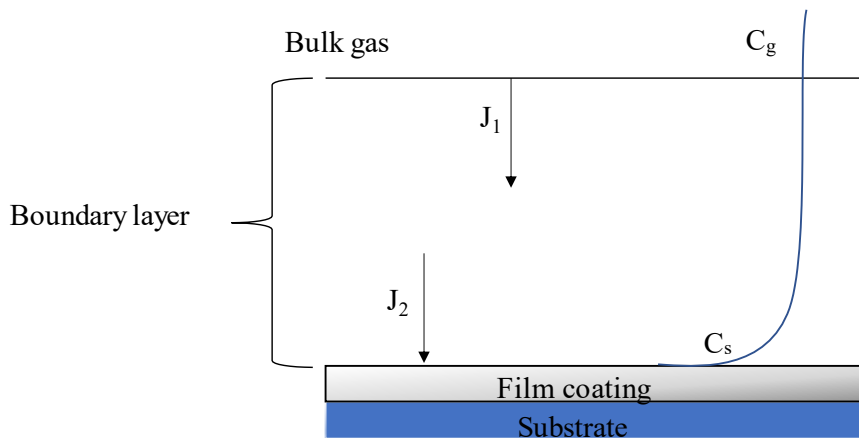


Figure 1.4 Schematic of growth process model in CVD

1.6 Common CVD reactors and mode of operation

There are different kinds of reactors for CVD applications, just as CVD techniques are often conveniently named after the pressure the deposition takes place or the source of energy. CVD reactors are also named according to their architecture, by process²¹ or by the number of substrates (wafers) a reactor can process at one time. Commercial reactors can be classified as either single-wafer or batch type²². A batch type reactor offers economies of scale in throughput, while single-wafer reactors frequently offer better process control from one wafer to the next. By architecture, the following are the kind of CVD reactors currently available:

- Tube reactors
- Showerhead reactors
- High-density plasma reactors
- Linear injection reactors

By process, the following are the kind of CVD reactors currently available:

- Atmospheric pressure CVD (APCVD)

- Low pressure CVD (LPCVD)
- Metalorganic CVD (MOCVD)
- Photon (Laser) induced CVD (PHCVD)
- Plasma enhanced CVD (PECVD)

The Table 1.2 below shows the type, distinguishing features, and commonly grown films according to this classification²².

1.6.1 Tube reactor: This kind of reactor is also known as a ‘hot-wall design reactor’, and this is simply because the walls of the tube are heated during deposition with the aid of resistive heaters. This reactor can be horizontally or vertically oriented, and it is very suitable for batch processing of wafers/substrates. One of the characteristic features of this type of reactor is that the films produced have good radial uniformity to achieve an axial uniformity as seen in Figure 1.5.

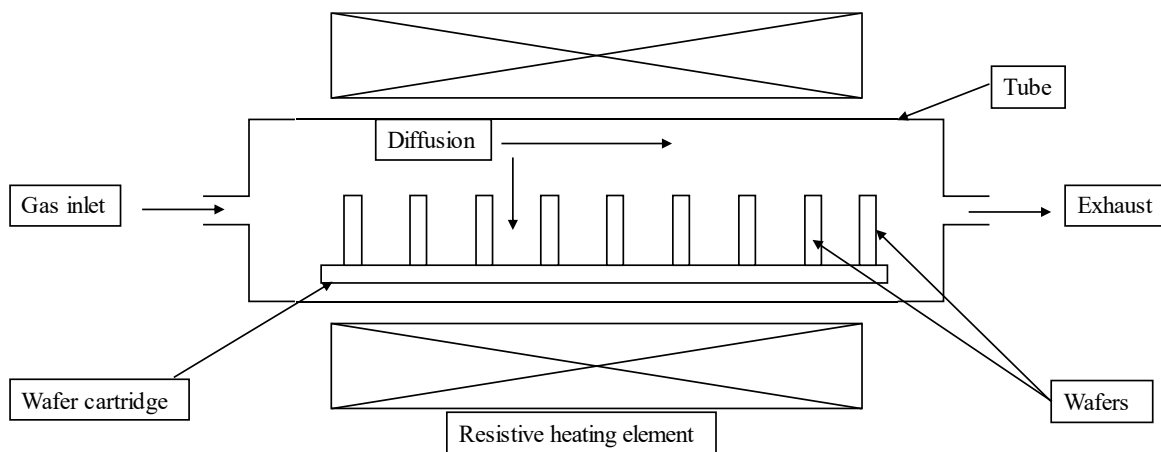


Figure 1.5 Schematic diagram of the tube reactor

Table 1.2 Classification of reactors and distinguishing features²²

Type	Distinguishing features	Commonly grown films
Single wafer	Process control	Dielectrics, metals
Batch	High throughput	Epi, oxides, W, WSi _x
APCVD	High rate	Doped oxides, epi
LPCVD, RPCVD	Process control, uniformity	Dielectrics, W, WSi _x , poly
Hot wall	Isothermal	Epi, TiN, poly, nitride
Cold wall	No deposition on walls	W, oxides
Chamber shape	Tube	Poly, doped oxides, nitride
	Pancake	Epi, poly
	Barrel	Epi

1.6.2 Showerhead reactor: The name showerhead reactor comes from the fact that the precursor gases for this reactor are being delivered into the system overhead as opposed to the tube reactor's which is being delivered side-to-side or end-to-end. This kind of reactor is also known as a 'cold-wall design reactor', and this is simply because only the substrate/wafer is heated during deposition with the aid of resistive heaters. It is well suited for plasma-enhanced processing²¹ with excellent radial uniformity as seen in Figure 1.6.

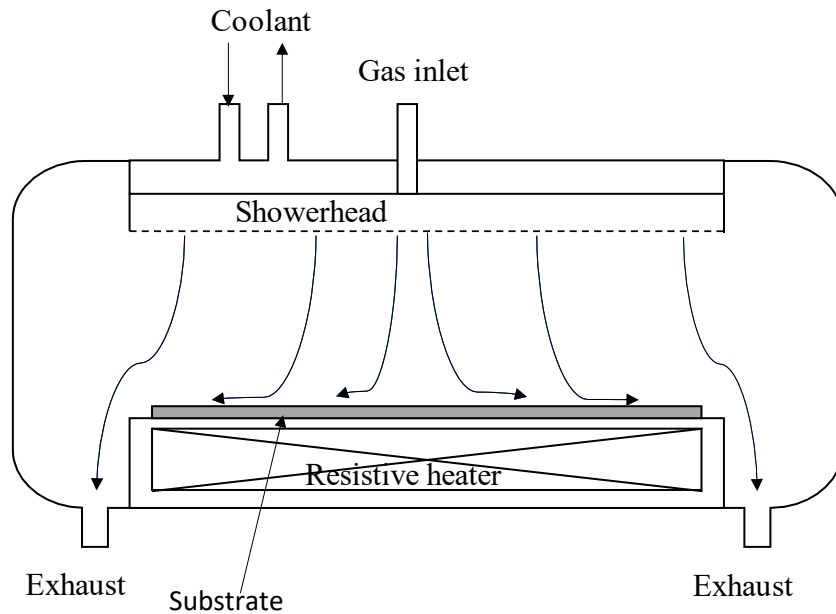


Figure 1.6 Schematic diagram of the showerhead reactor

1.7 Objectives of the thesis

Carbon based materials (CBMs), and more specifically 2D materials graphene have been developed via various physical and chemical means. Some of these processes are energy intensive-using graphene as a point of reference, and it has been reported by most literatures to be thermally grown at 1000°C or more using CVD technique. The aim of this thesis is to explore possibility of growing CBMs at lower energy requirements using a novel laser-assisted CVD technique. We plan to accomplish this by constructing a laser-assisted CVD system by incorporating a laser source, mass flow controllers (MFCs), a gas source, a resistant heater, and a vacuum system. With this, we determine how parameters like temperature, CH₄ flow rate, and laser frequency affect the growth of CBMs.

EXPERIMENTAL

2.1 Design and engineering

2.1.1 General construction: The construction and design of the custom-built laser-assisted chemical vapor deposition (CVD) chamber shown in Figure 2.1 below was spearheaded by the author of this thesis with the help of those named in the acknowledgement section. The principal components of this system are: a traditional PLD chamber, a solid state Nd: Yag laser of wavelength 266nm, mass flow controllers (MFC), a roughing and turbomolecular pump, a baratron gauge, a bourdon gauge, a heater, a temperature controller, a UV mirror, a network of gas supply lines, and the precursor gases.

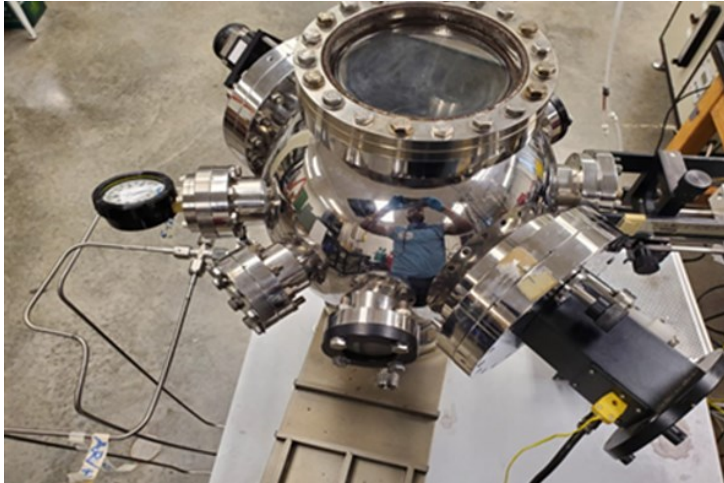


Figure 2.1 Custom-built laser-assisted CVD chamber

2.1.2 Equipment (working principles): Here we look at the working principles of all the equipment used in carrying out this experiment. In this section, we will share a brief account of how this works. We will consider the work done under three headings listed below:

- Gas flow assembly
- Optical assembly
- Heating system

2.2 Gas flow assembly

In this section, we get to address the mass flow controller system, the vacuum pump system, and their principle of operation.

2.2.1 Mass flow controllers (MFC): Here we have 2 gas lines supplying our precursor gases: a single line carrying methane and the other carrying a mixture of hydrogen and argon gas.

These mass flow controllers consist of a sensor, bypass and flow rate control valve which work simultaneously to measure and control the flow rate. As the gas flows in from the inlet, it is made to flow past a flow rate sensor and a bypass. The primary function of the sensor is to measure the mass flow rate of the gas, and the presence of a flow rate control valve serves as a modulator using the difference between the measured flow rate and the flow rate received from the external flow rate signal setting²³.

The gas, which enters from the inlet, is channeled to flow past the sensor or the bypass. The sensor measures the mass flow rate as a function of change in temperature and then converted by the bridge circuits to an electrical signal as seen in Figure 2.2. This signal is amplified and corrected through the amplification and correction circuits which outputs it as a linear voltage between 0 to 5V and simultaneously sending it to the control circuits for comparison. This compares the flow rate setting signal, and the actual flow setting signal from the sensor and a difference signal is sent to the valve driving circuit. The flow rate control valve

moves in proportionately to accommodate the difference between the required flow set point and flow output signals approach zero.

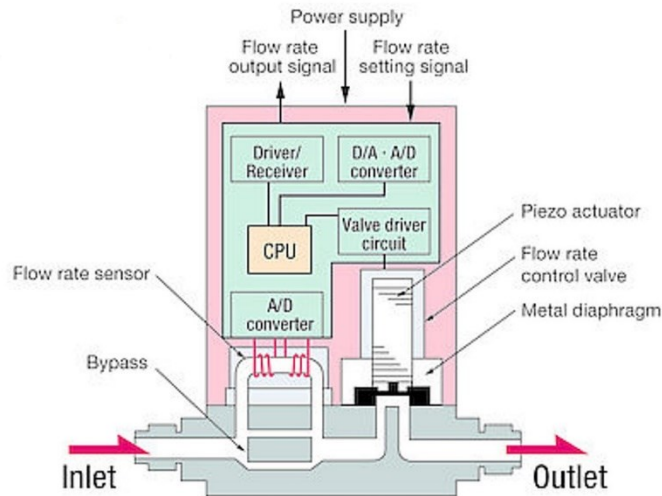


Figure 2.2 Schematic diagram of a mass flow controller (MFC)²³

The gas flow using the MFCs can be made to flow individually or as a ratio of one gas flow rate to the other. The MKS type 247D four-channel mass flow controller was used in this case. The 247 unit has four signal conditioning channels, four set point circuits, and a digital panel meter (DPM) to show the real-time flow rate of the selected channel of any of the MFCs as seen in Figure 2.3 and Figure 2.4. Using this device, the gas flows can either be set independent of one another or as a ratio to a reference gas/flow line as one may wish²⁴.

The pictures in Figure 2.3 and Figure 2.4 below show the MKS type 247D four-channel mass flow controller front and rear panel controls. Some of these functions will be addressed subsequently. For this process, we decided to make use of manual flow control therefore using only the MFC interface cables and primarily control the individual flow rate for each gas from

the front panel set point control. In addition, one can decide to control as many as four gas lines with the aid of the MFC connectors (J1 - J4) on the rear panel.

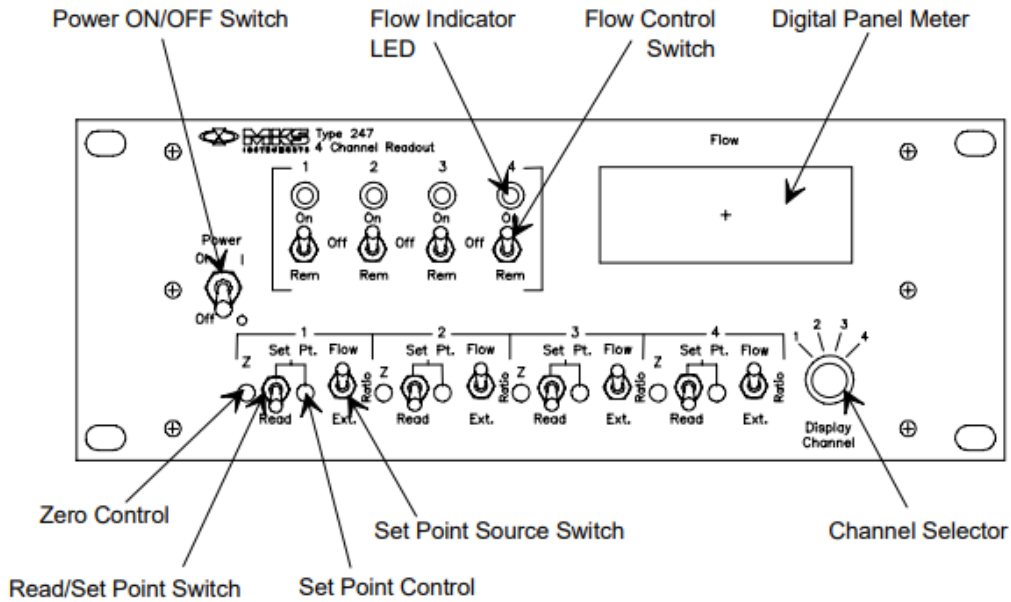


Figure 2.3 Front panel controls²⁴

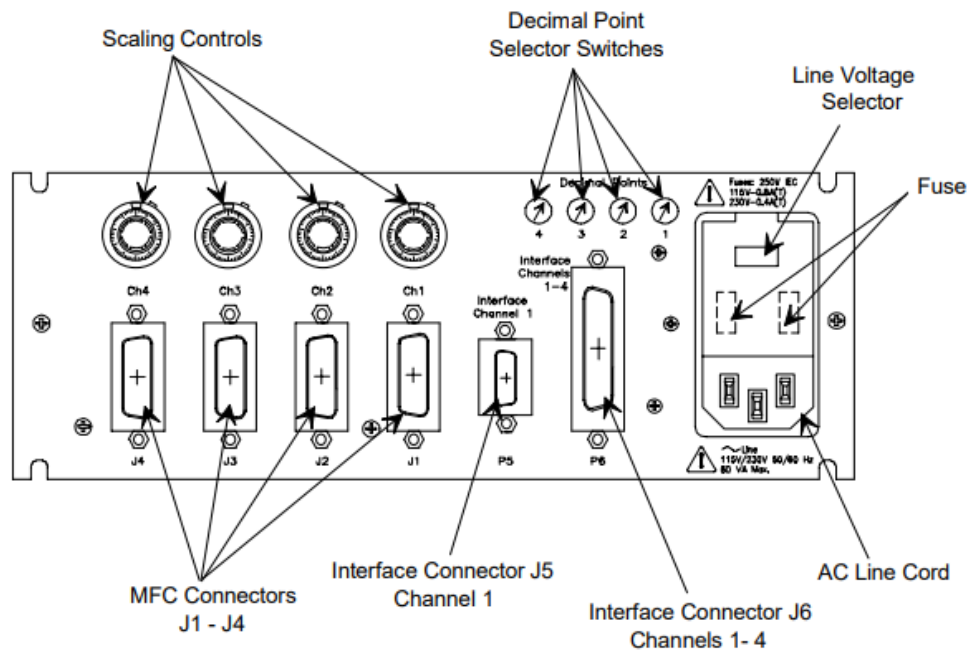


Figure 2.4 Rear panel controls²⁴

To adequately flow a gas using the MKS type 247D four-channel MFC, we need to understand a few terms:

- Gauge factor
- Gas correction factor
- Scaling control factor (SCF)

2.2.1.1 Gauge factor: This is a factory set value which scales the +5V DC output signal to the appropriate full-scale range for the MFC, so that the digital display panel reads 1000 counts. The gauge factors for various flow ranges are listed in Table 2.1 below.

Table 2.1 MFC gauge factors²⁴

MFC gauge factors	
MFC flow range (sccm)	Gauge factor
1, 10, 100, 1000, 10000	100
2, 20, 200, 2000, 20000	200
5, 50, 500, 5000, 50000	50

2.2.1.2 Gas correction factor (GCF): This value is used to show the ratio of flow rates of different gases that will yield the same output voltage from an MFC. This value relies on a host of factors like specific heat, density, and the molecular structure of the gases. The baseline gas is nitrogen, and a value of 1 is assigned to it as its nominal value. The GCF of some common gases can be found in ref²⁴. Alternatively, the GCF of a pure gas or mixture of gases can be calculated thus²⁴:

For pure gases,

$$GCF_x = \frac{(0.3106)(s)}{(d_x)(cp_x)}$$

where:

GCF_x = Gas correction factor for gas X

0.3106 = (Standard density of nitrogen) (Specific heat of nitrogen)

s = Molecular structure correction factor where s equals:

1.030 for monatomic gases

1.000 for diatomic gases

0.941 for triatomic gases

0.880 for polyatomic gases

d_x = Standard density of gas X, in g/l (at 0° C and 760 mmHg)

cp_x = Specific heat of gas X, in cal/g° C

For a mixture of gases,

$$GCF_x = \frac{(0.3106)(a_1s_1 + a_2s_2 + \dots + a_ns_n)}{(a_1d_1cp_1 + a_2d_2cp_2 + a_nd_ncp_n)}$$

where:

GCFM = Gas correction factor for a gas mixture

0.3106 = (Standard density of nitrogen) (Specific heat of nitrogen)

a_1 and a_2 = Fractional flow of gases 1 and 2

Note: a_1 and a_2 must add up to 1.0

s_1 and s_2 = Molecular structure correction factor for gases 1 and 2

where s equals:

1.030 for monatomic gases

1.000 for diatomic gases

0.941 for triatomic gases

0.880 for polyatomic gases

d_1 and d_2 = Standard densities for gases 1 and 2, in g/l

(at 0° C and 760 mmHg)

cp_1 and cp_2 = Specific heat of gas 1 and gas 2, cal/g° C

Since the gas used here is CH₄ and Ar/H₂ (95% Ar, 5%H₂) gases, we can calculate their GCF as:

$$GCF_{methane} = \frac{(0.3106)(0.88)}{(0.715)(0.5328)} = 0.7175$$

And for the Ar/H₂ gas mixture, we can say:

$$GCF_{mixture} = \frac{(0.3106)((0.5 \times 1.030) + (0.5 \times 1))}{(0.5 \times 1.782 \times 0.1244) + (0.5 \times 0.0899 \times 3.419)} = 1.1918$$

2.2.1.3 Scaling control factor (SCF): This is simply the product of the gauge factor for the MFC in use and the GCF for the gas in use:

$$SCF = Gauge\ factor \times GCF$$

The value of the SCF is then set on the scaling control potentiometer dial. The SCF value changes as we choose a new flow rate under the guidance of the gauge factor. The gas flow rate is then set on the front panel and we can choose to flow the gases in succession like we did in our experiment.

2.2.2 Vacuum system: A vacuum system comprising of a roughing pump and a turbomolecular pump connected in series was used for pumping gas out of the deposition chamber at a base pressure of 5E-5 Torr. The primary function of the roughing pump is to

initially pump down the chamber from atmospheric pressure to a low enough pressure within the operating range of the turbomolecular pump, afterwards, it reverts to a secondary position where it supports the turbomolecular pump by providing a low enough pressure at the outlet. Figure 2.5 shows a schematic diagram of the roughing/rotary vane pump.

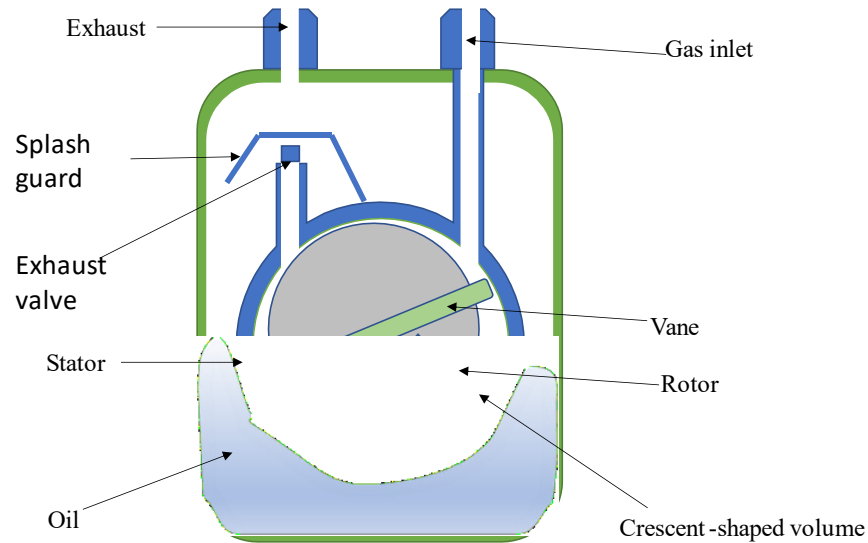


Figure 2.5 Schematic diagram of the roughing/rotary vane pump

By design, the rotary vane pump has its rotor mounted eccentrically in the body of the stator with the vanes diametrically loaded on opposing sides of the rotor. The curvature of the vanes is designed to press against the internal walls of the stator wall by the central springs on which it rotates or by the centrifugal force induced at rotary motion. This pressing of the vanes on the rotor against the interior walls of the stator encases the gas into a confined volume²⁶. The deposition/vacuum chamber to be evacuated is connected to the inlet of the pump through a gate valve. When the pump is in operation, initially the pressures in the trapped region and in the system are equal, with time, the volume of the entrapped gas reduces, thereby causing

compression at higher pressure and then transported to the outlet port. The oil in the pump helps seal the joints from leaks, lubricate the moving parts and cool the pump assembly.

A turbo-molecular pump is simply a molecular pump that operates by means of momentum transfer from its high-speed rotating blades to the gas molecules. It consists of a rotor of discs with conveying channels. The gas molecules are compressed as the discs rotate between corresponding discs of the stator. Turbo-molecular pumps can either be classified as single or double-flow turbo-molecular pumps²⁷. Modern turbomolecular pumps are designed as single-flow systems, meaning that, the first high-vacuum stage is situated below the suction flange to reduce conductance losses.

The high-speed rotating blade surfaces of the turbomolecular pump are machined angled slots directed radially inwards from the edge of a circular disc to form a bladed rotor as seen in Figure 2.6. The rotors turn at speeds sufficient to give their outer parts velocities comparable with molecular velocities. The rotors have an alternating arrangement with an identical set of stator blades that directs inwards from the wall of the cylindrical pump encasement²⁸.

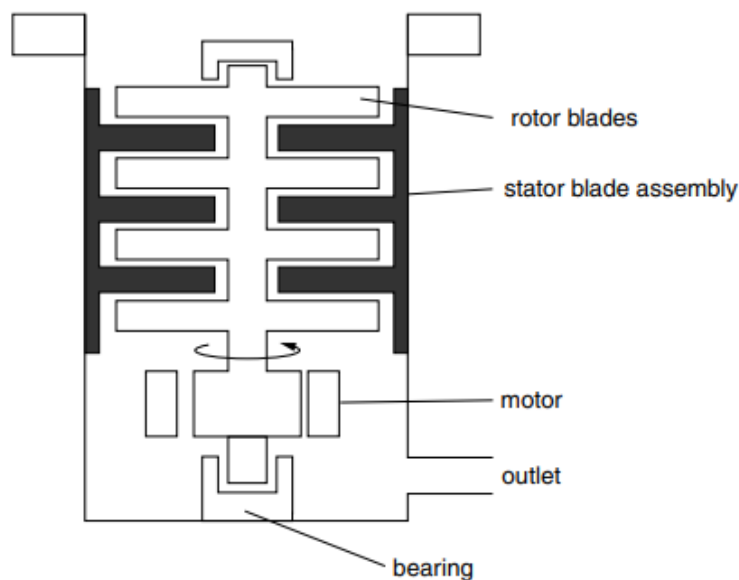


Figure 2.6 Schematic diagram of the turbomolecular pump²⁸

2.3 Optical assembly

In this section, we get to talk about the Nd:YAG laser (its principle of operation), UV mirrors, and the roles they both played in our experiment.

2.3.1 Nd: YAG laser: Simply put Nd:YAG laser means Neodymium-doped Yttrium Aluminum Garnet ($Y_3Al_5O_{12}$). It is a solid state laser, and because the terminal level is well above the ground-state multiplet, the Nd:YAG operates as a four-energy level laser system²⁹, that is, the four energy levels are involved in laser action which may be designed in both pulsed and continuous mode.

For this kind of laser, the laser medium is the Nd: YAG crystal. The pumping method employed in this laser is optical pumping - a process in where light is focused unto a specimen under study and the effect of the light on the specimen is analyzed³⁰. A xenon or krypton flash tube is used as pumping source (but diodes are used in more recent designs for increased efficiency and low cost) since the difference in the energy levels causes the electrons to require some external pumping for a transition from one energy state to the next.

An optical resonator is made from both ends of Nd: YAG rod by polishing it with silver (one end is fully silver-coated and the other, partially) as seen in Figure 2.7. The fully silvered end acts as a fully reflecting mirror and completely reflects the light while the partially silvered end allows a small portion of light through it to produce the laser beam³¹.

The resulting wavelength of the output beam of the Quantel Q-smart Nd:YAG pulsed laser used is for our experiment is 266nm.

The reason why the laser was used is to act as a secondary energy source for our laser-assisted CVD process. This was done by making the pulsed laser beam incident on the copper and silicon substrate with the aid of a 248nm UV mirror, while the heat from the resistive heater

serves as the primary source of energy simultaneously. The Figure 2.8 below shows a simple process of how this was done.

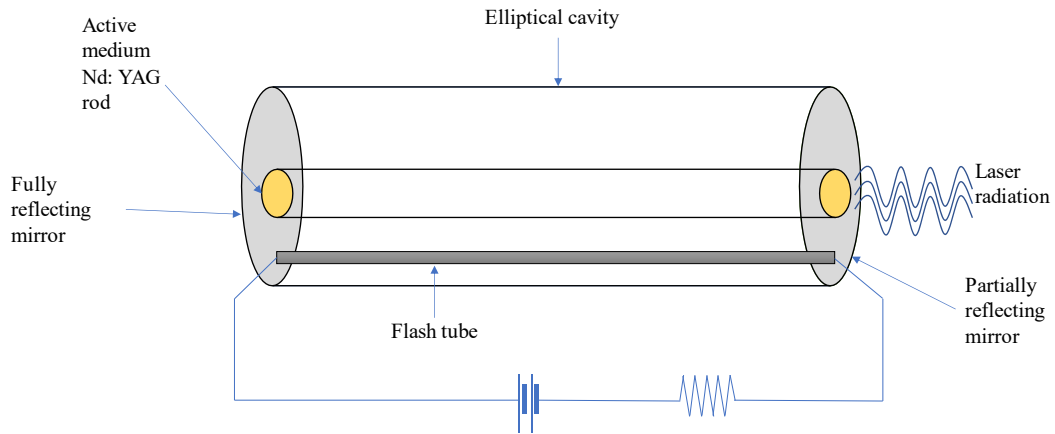


Figure 2.7 Schematic diagram of the Nd:YAG laser

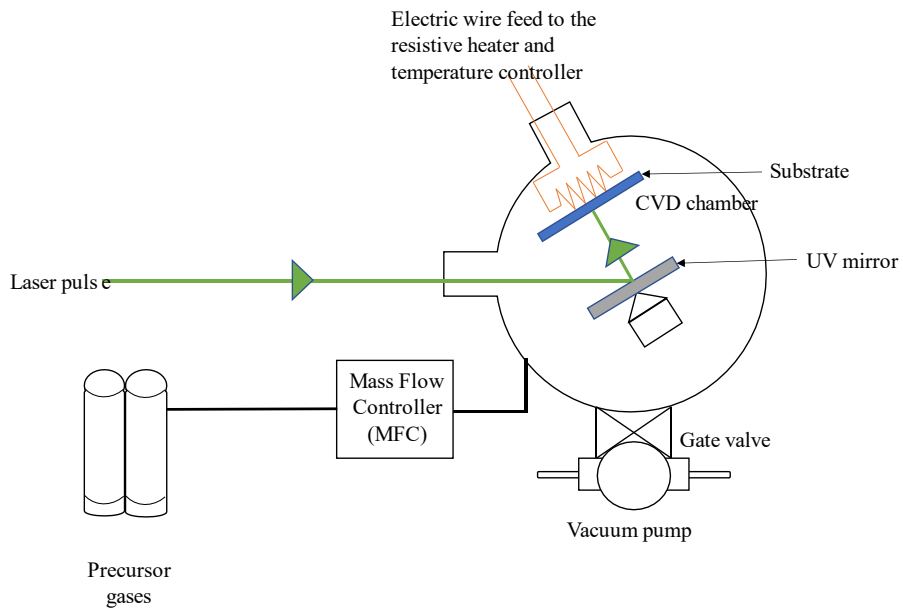


Figure 2.8 Schematic diagram of the deposition process in the chamber

2.4 Heating system

For our experiment, we designed two systems as our primary sources of heating, the first is the use of resistive heating in the chamber and the second is inductive heating using a quartz tube in an induction furnace. This inductive heating system was designed so that we can replicate experiments done via resistive heating and to attempt the deposition at higher temperatures impossible by the former. We will touch briefly on the difference between these two methods of heating.

Resistive heating occurs when the energy of an electric current is converted into heat as it flows through a medium of finite conductivity in which electrical energy is converted to heat through resistive losses. This mode of heating describes a process of heat generation by virtue of the collision between the conduction electrons and the conductor's atoms during energy transfer³³.

In contrast, induction heating is a non-contact heating process that involves heating a conductor by electromagnetic induction, causing eddy currents to be generated in the metal and resistance leads to Joule heating of the metal. An induction heater is made up of an induction coil through which a high frequency alternating current (AC) is passed with the generation of a time-varying magnetic field, typically, only metals with high electrical conductivity can be heated via this method. Magnetic hysteresis losses may also contribute to heat generation in some materials³⁴. Figure 2.9 and Figure 2.10 show the various heating equipment used.



Figure 2.9 Resistive heater and vertical furnace

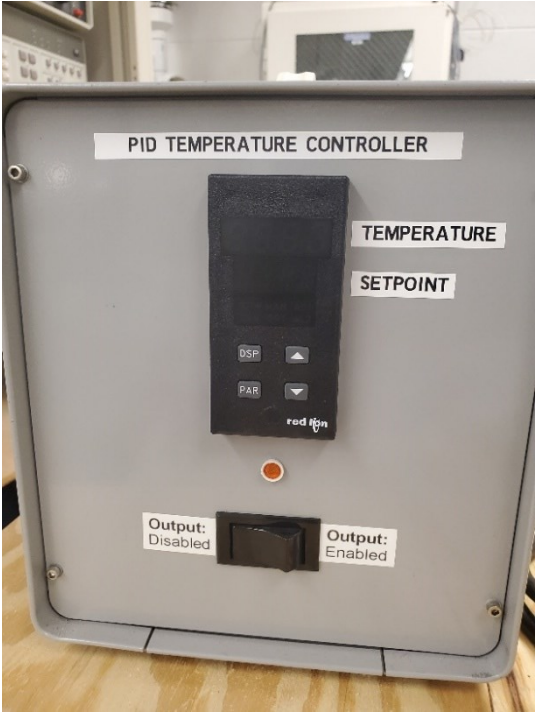


Figure 2.10 PID temperature controller

2.5 Sample preparation and process flow

2.5.1 Sample preparation: We start our sample preparation by sonicating copper and silicon substrates in acetone in different beakers (for 15 minutes). Acetone is a very good polar solvent and dissolves almost all organic compounds that may be found on the substrates. However, upon careful examination, acetone leaves a residue on substrates. Therefore, we need to remove it using Iso-Propyl-Alcohol (IPA). We then rinse with water to wash away the IPA and any inorganic salts found on the substrates, afterwards., We finally rinse in methanol to displace any water at might have adhered to the substrates.

To clean the resistive heater in which our substrates would sit, we first rub it with a coarse sandpaper, then a fine one and then employ a similar method we used in cleaning our substrate for the resistive heater. A similar technique was used to clean the quartz tube of the vertical tube furnace.

2.5.2 Process flow: The laser-assisted CVD system was put together by connecting gas bottles to the MFC and then to the deposition chamber through a series of inter-connected stainless-steel pipes and valves. The gas lines were vacuum tested using a baratron capacitance manometer to ensure there were no gas leaks. The deposition chamber is connected to a vacuum pump (roughing and turbomolecular) through a gate valve. The pumping pressure was read on the display panel meter, and the deposition pressure was measured using a bourdon gauge and a capacitance manometer. The gas flow set-up was identical for both the resistive heater and the tube furnace experiments, Figures 2.11 and 2.12 shows their P&ID chart.

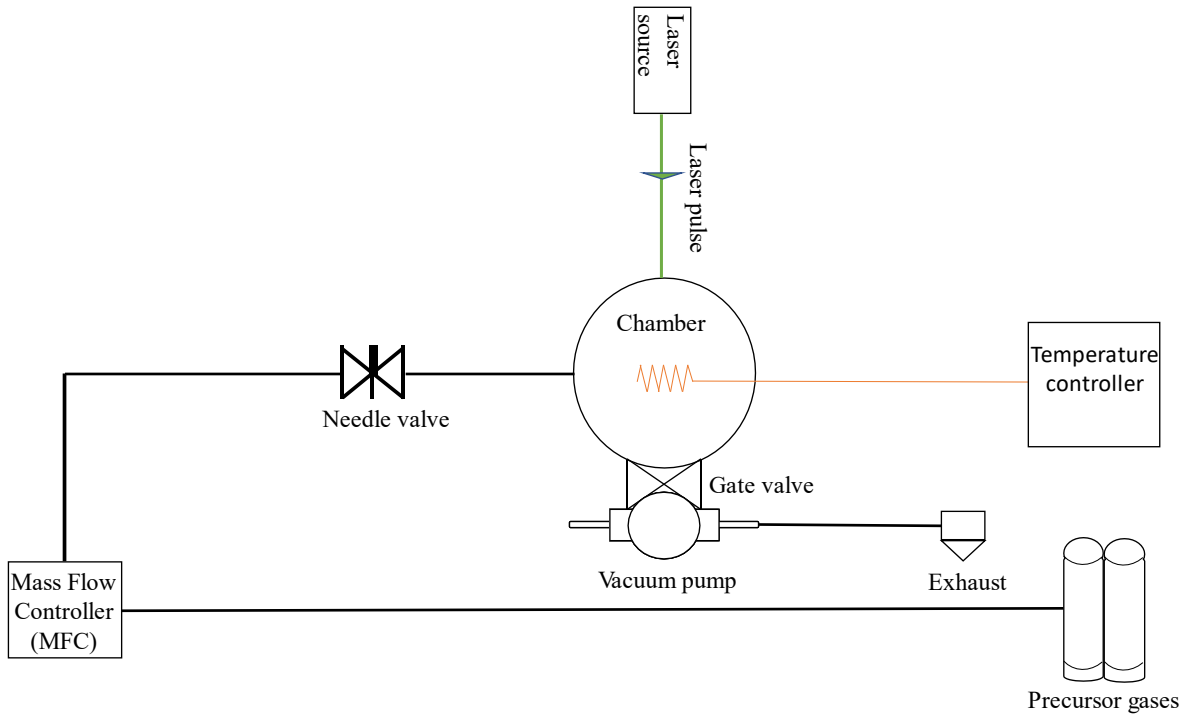


Figure 2.11 P&ID chart for laser-assisted CVD via resistive heating

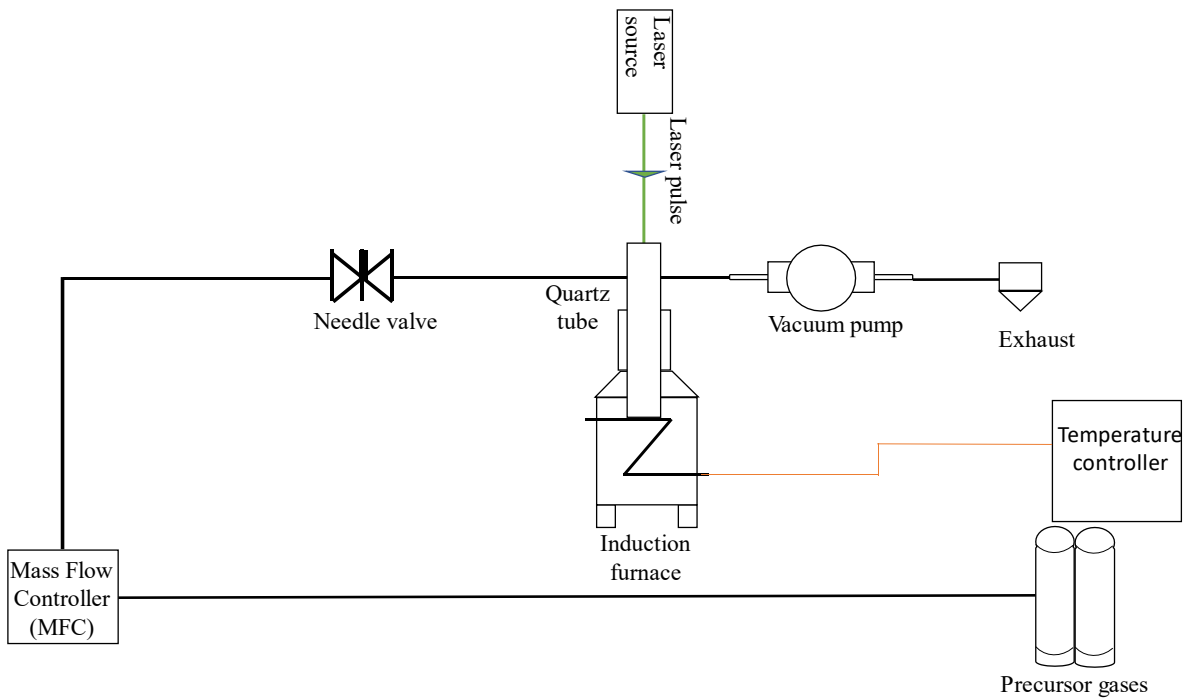


Figure 2.12 P&ID chart for laser-assisted CVD via inductive heating

To initiate a deposition, the substrates are placed in the deposition chambers, and it is being pumped down from atmospheric pressure to about 5×10^{-5} Torr. Then we begin to introduce Ar/H₂ (buffer gas) gas at the required flow rate using the programmed MFC. Once we notice a pressure build up from the bourdon gauge, we turn on the PID controller and anneal the substrates to prevent dewetting. Once this is done, we used some laser pulses (of some few hundreds or thousands) to clean the substrates. As the laser pulses are being directed onto the substrate with the aid of the UV mirror, at the required deposition pressure and temperature, we shut-off the buffer gas and turn on the CH₄ (carbon source) from the front panel of the MFC. The role of the buffer gas is just to add pressure into the system. During the time of deposition, the pressure and temperature are both maintained, and the pulsed laser runs simultaneously as the methane is being pumped into the chamber. The pulsed laser is meant to serve as a secondary source of energy to break the carbon-hydrogen bonds of the methane.

After deposition is complete, the laser is turned off, the gas is shut off and the substrate is allowed to cool in the chamber.

2.6 Characterization

In this section, we consider the underlying principles of the various characterization techniques used to study the CBMs grown in the laboratory.

2.6.1 Raman spectroscopy: This works based on the interaction between light and matter. When monochromatic light incidents on a material it might be reflected, absorbed, or scattered. It is this scattering feature we exploit when performing Raman spectroscopy. When a sample is excited as seen in Figure 2.12, three modes of scattering are created, Rayleigh (elastic), Raman stokes (inelastic), and Raman anti-stokes (inelastic), during which this time, a very short-

lived unstable state between the photon and molecule is created called the virtual state of the molecule and at this instance, the photon is re-emitted as scattered light. Only a small amount of this scattering is Raman (about 0.0000001%), depending on the molecular structure of the sample³⁵.

If the emitted radiation is of lower frequency than the incident radiation, it is called Stokes scattering and if it is of higher frequency, then it is called anti-Stokes scattering. If it is the same, it is Rayleigh scattering as shown in Figure 2.13 and Figure 2.14. Quantum mechanically, both types of inelastic scattering are equally probable, but statistically speaking, Stokes scattering is more likely hence, the Stokes scattering is way more intense than the anti-Stokes and oftentimes, Stokes scattering is more utilized³⁶.

Raman spectroscopy is useful in so many ways: it provides information on chemical structure and phase identification, polymorphism, bond interaction as it relates to stress/strain, doping and impurity study, the relative quantity of material, defect analysis, crystallinity, molecular bond vibration and interaction, and studying low frequency vibrational modes of molecules, study of single-walled carbon nanotubes (SWCNTs).

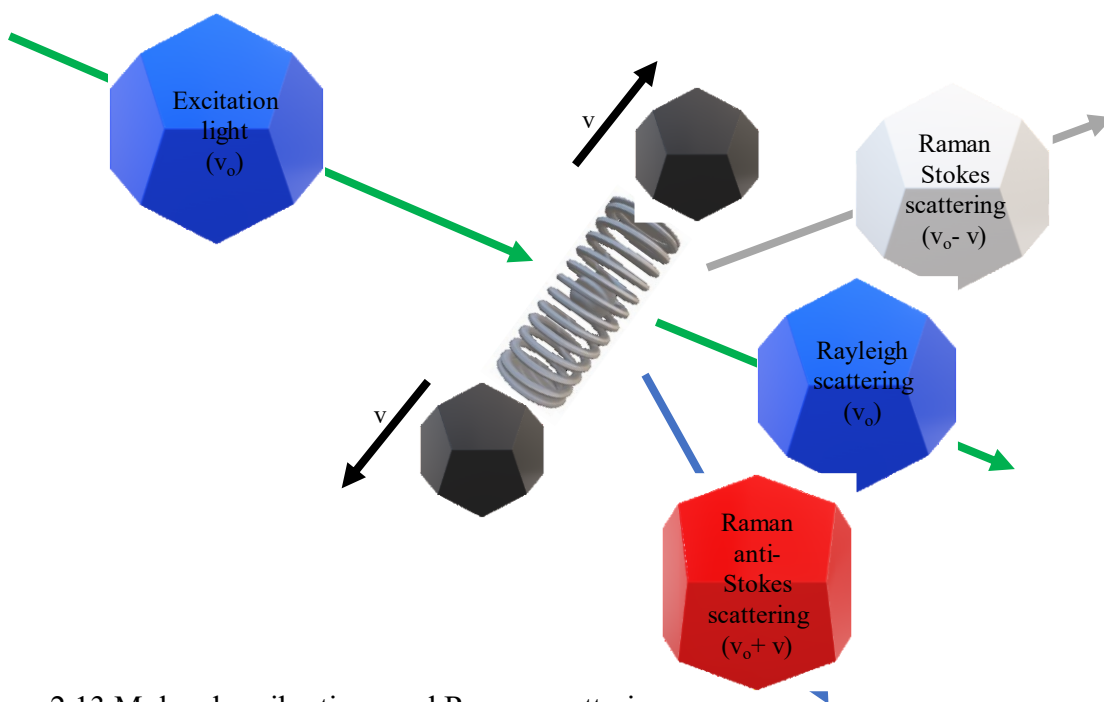


Figure 2.13 Molecular vibrations and Raman scattering

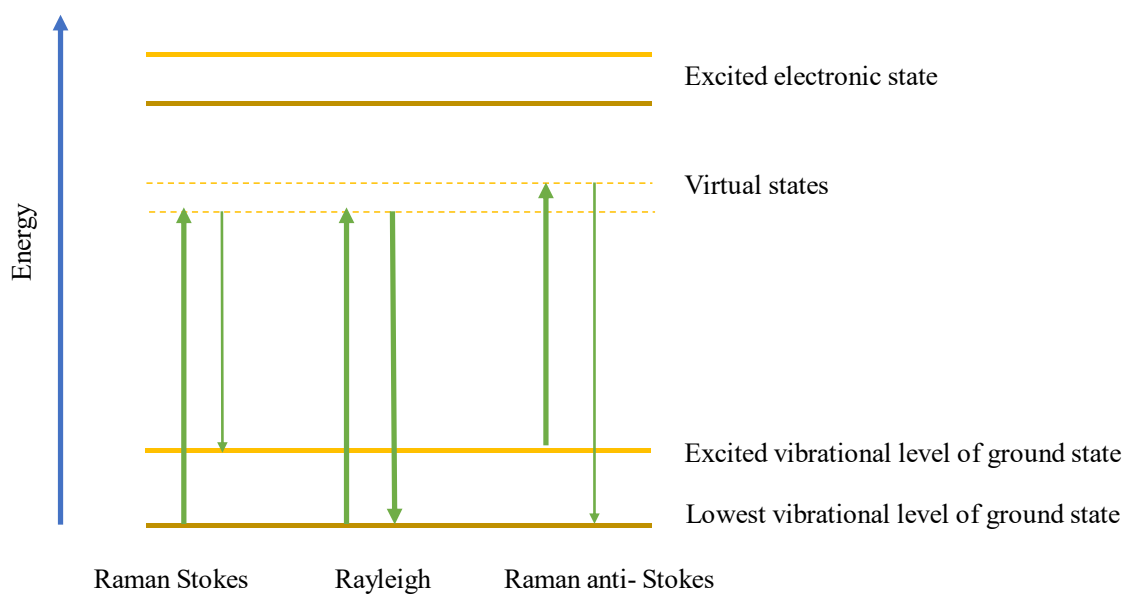


Figure 2.14 Diagram of the Rayleigh and Raman scattering processes

RESULTS AND DISCUSSION

3.1 Data presentation and analysis

Here, we present our data, interpret, and discuss what they mean. The substrates used are silicon dioxide wafer ($\text{Si}_{x,y}$) and copper foil ($\text{Cu}_{x,y}$), where x represents the sample number and y is 0 when there is no laser irradiation and 1 when there is laser irradiation. The deposition pressure was 550 Torr, Ar/H₂ flow rate was set to 10 sccm and the energy density was calculated to be 0.116J/cm² per pulse. Si₁ and Cu₁ represent the pristine silicon wafer and copper foil at room temperature without the presence of laser shots. The Table 3.1 below shows the process parameters for the laser-assisted CVD of our carbon-based material via the resistive heating process on both silicon and copper substrates.

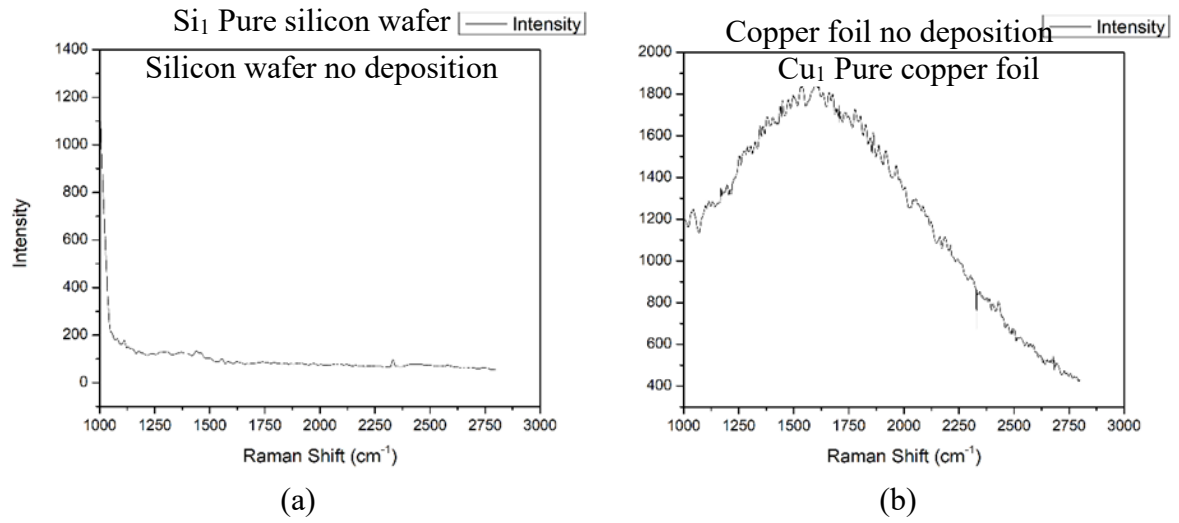
Before we proceed, I would like to share three Raman plots showing the spectra for pure silicon substrate without any deposition, pure copper substrate without any deposition, and a commercial grade graphene obtained from the Airforce Research Laboratory as seen in Figures 3.1 (a-c). We will refer to them later in this text.

In this thesis, we varied four parameters, namely:

1. CH₄ flow rate
2. Temperature
3. Substrate
4. Time.

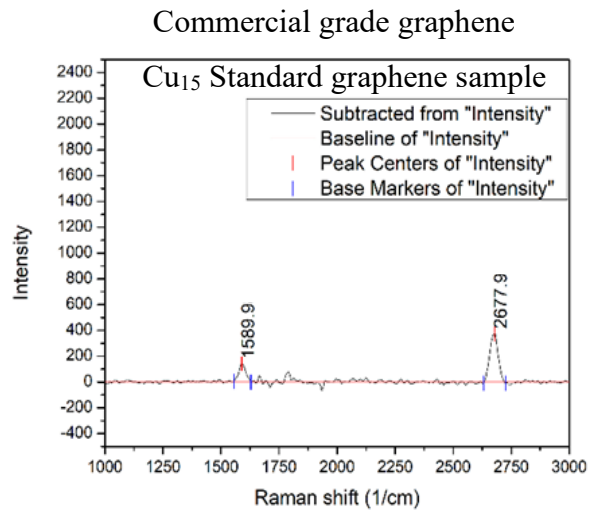
Table 3.1 Process parameters for silicon and copper substrate via resistive heating

Sample ID		Process parameters			
		Temp (°C)	Laser pulse frequency (Hz)	CH ₄ flow rate (sccm)	Deposition time (min)
Si ₁	Cu ₁	25	-	-	-
	Cu _{2,0}	650	5	10	5
	Cu _{2,1}	650	5	10	5
	Cu _{3,0}	650	10	20	5
Si _{3,1}	Cu _{3,1}	650	10	20	5
	Cu _{4,0}	700	5	10	5
	Cu _{4,1}	700	5	10	5
	Cu _{5,0}	700	10	20	5
Si _{5,1}	Cu _{5,1}	700	10	20	5
	Cu _{6,0}	750	5	10	5
	Cu _{6,1}	750	5	10	5
	Cu _{7,0}	750	10	20	5
Si _{7,1}	Cu _{7,1}	750	10	20	5
	Cu _{8,0}	800	10	10	5
	Cu _{8,1}	800	10	10	5
	Cu _{9,0}	800	10	20	5
Si _{9,1}	Cu _{9,1}	800	10	20	5
	Cu _{10,0}	850	5	10	5
	Cu _{10,1}	850	5	10	5
	Cu _{11,0}	850	10	20	5
Si _{11,1}	Cu _{11,1}	850	10	20	5
	Cu _{12,0}	850	10	20	3
	Cu _{12,1}	850	10	20	3
	Cu _{13,0}	850	10	20	1
	Cu _{13,1}	850	10	20	1
	Cu _{14,0}	850	0	20	5
	Cu ₁₅	Standard sample			



(a)

(b)



(c)

Figures 3.1 (a-c) Raman spectra of pristine silicon, copper, and high-quality graphene

3.2 Variation of CH₄ flow rate and temperature

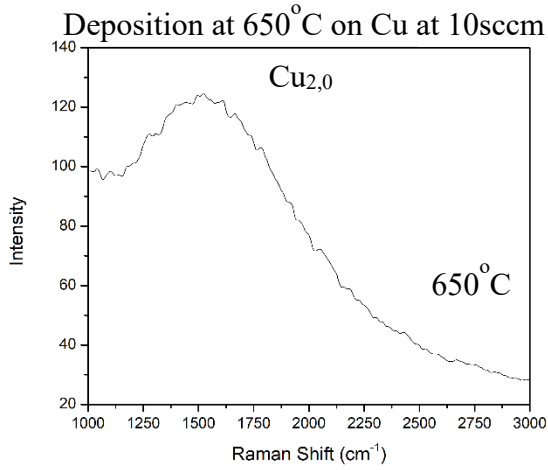
Deposition was done at two flow rates: 10sccm and 20sccm. We consider the effect of change in temperature for both flow rates as we ran our depositions between 650°C and 850°C.

3.2.1 Constant CH₄ flow rate at 10sccm and varied temperature: The Table 3.2 below shows a constant CH₄ flow rate of 10sccm and varied temperature with accompanied Raman spectra graphs in Figures 3.2.

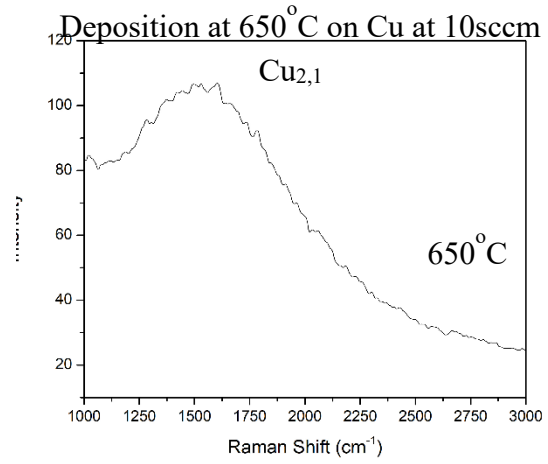
Table 3.2 Constant CH₄ flow rate at 10sccm and varied temperature

Sample ID	Process parameters			
	Temp (°C)	Laser pulse frequency (Hz)	CH ₄ flow rate (sccm)	Deposition time (min)
Cu _{2,0}	650	5	10	5
Cu _{2,1}	650	5	10	5
Cu _{4,0}	700	5	10	5
Cu _{4,1}	700	5	10	5
Cu _{6,0}	750	5	10	5
Cu _{6,1}	750	5	10	5
Cu _{8,0}	800	10	10	5
Cu _{8,1}	800	10	10	5
Cu _{10,0}	850	5	10	5
Cu _{10,1}	850	5	10	5

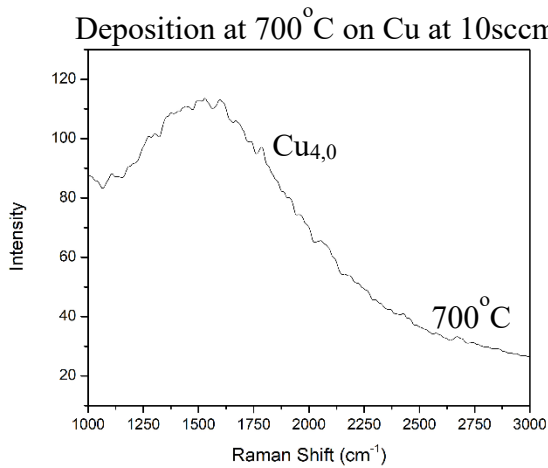
Here, we kept a constant gas flow rate and varied temperature between 650°C and 850°C using copper substrates, the laser frequency was also varied between 5 and 10Hz and a deposition time of 5 minutes.



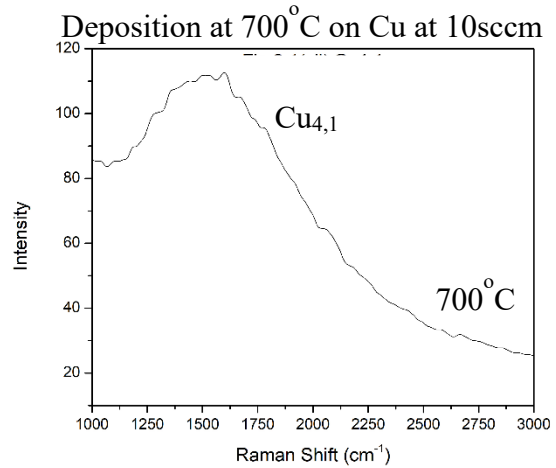
(a)



(b)

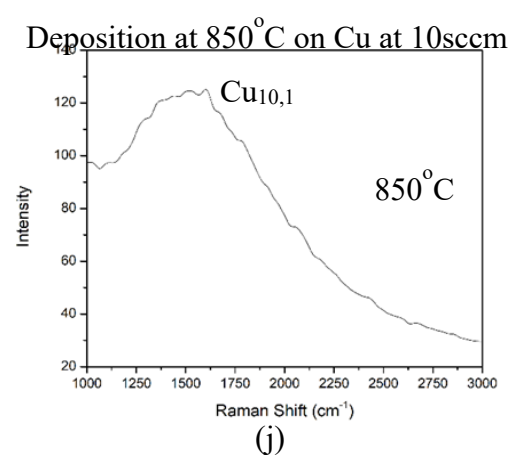
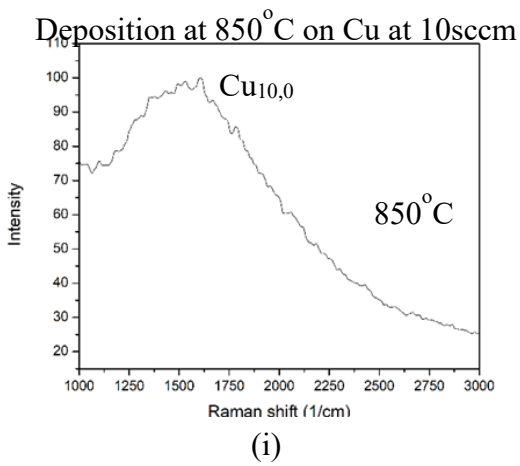
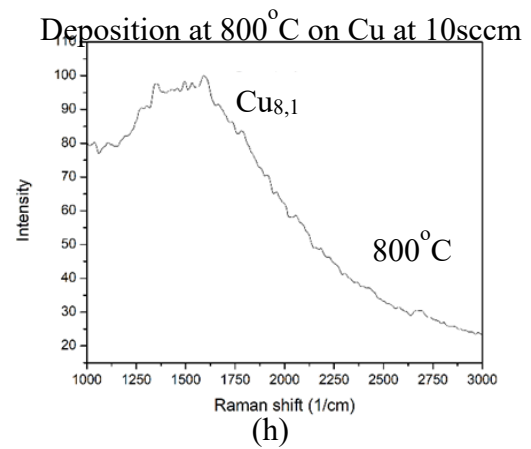
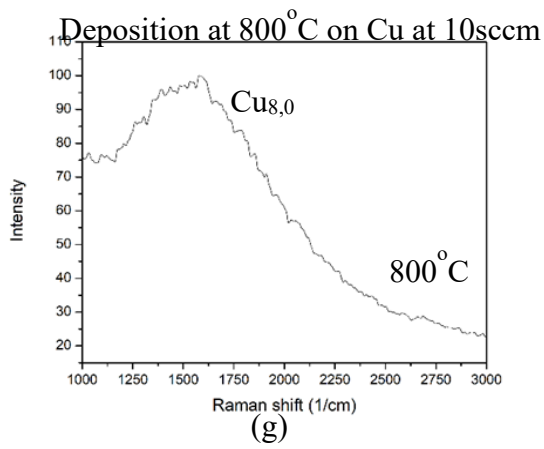
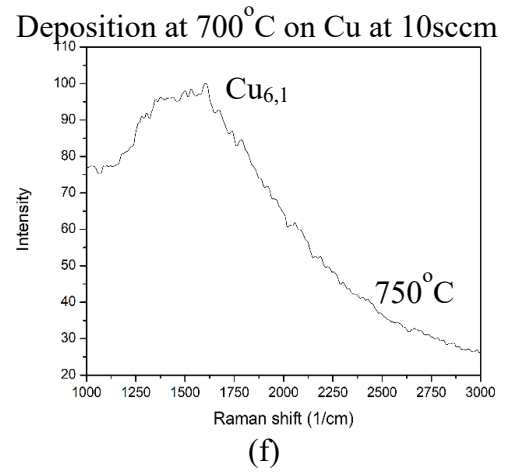
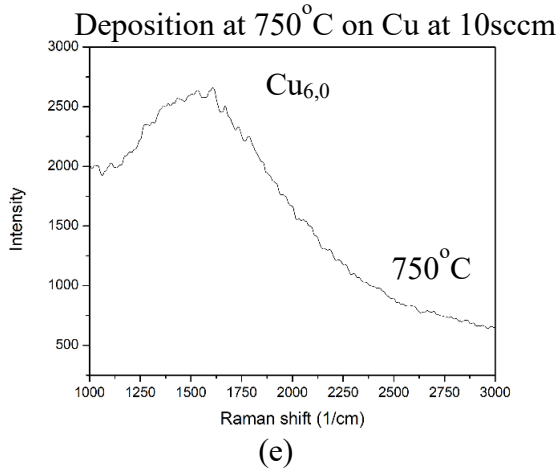


(c)



(d)

Figures 3.2 (a-d) Raman spectra at constant CH_4 flow rate at 10sccm and varied temperature



Figures 3.2 cont'd (e-j) Raman spectra at constant CH_4 flow rate at 10sccm and varied temperature

It can be observed that there were no distinguishable peaks to indicate growth, this led us to make two plausible assumptions:

1. From Grove's model, the mass transport of the reactant gaseous species across the boundary layer only depends on the mass diffusion. Hence, there is a concentration gradient of the gaseous species, and the flux of mass transport from the gas phase, and the substrate surface is insufficient to initiate the required reaction. This means that the set flow rate of 10sccm is too low for deposition to take place.
2. The temperature needed to thermally break the carbon-hydrogen bonds at the required dehydrogenation energy was not reached.

Assumption 1 prompted us to increase the methane flow rate to 20sccm and repeat the experiment.

3.2.2 Constant CH₄ flow rate at 20sccm and varied temperature: The Table 3.3 below shows a constant CH₄ flow rate of 20sccm, frequency of 10Hz and varied temperature with accompanied Raman spectra graphs in Figures 3.3 for both silicon and copper substrates.

We can observe that for the silicon graphs below, there is no distinguishable peak to show deposition of any form of CBM in crystalline form, for the copper substrate there were no identifiable peaks at 650°C but faint ones at 700°C. However, at 750°C on the laser incident part of our sample, we noticed three peaks at the Raman shift of 1351.8cm⁻¹, 1585.5cm⁻¹, and 2702.3cm⁻¹, they are D, G and 2D peaks respectively, the signature peaks for carbon-based material like graphene.

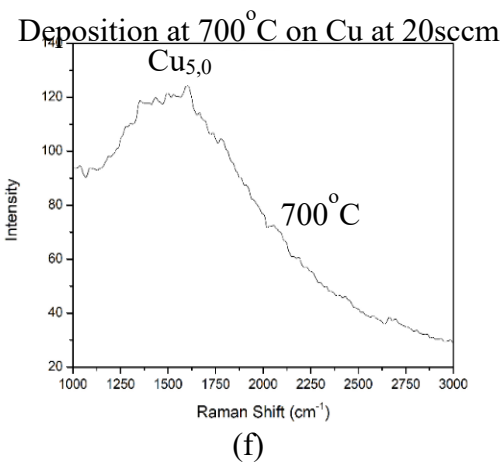
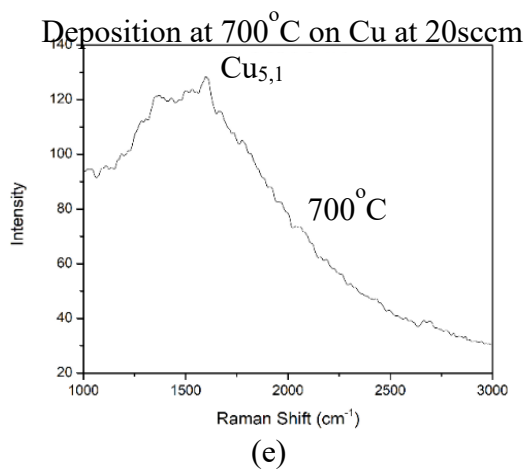
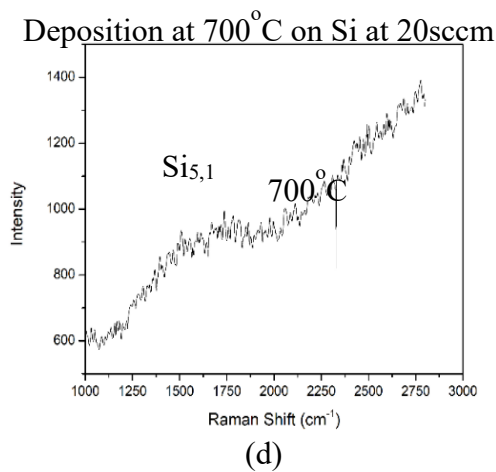
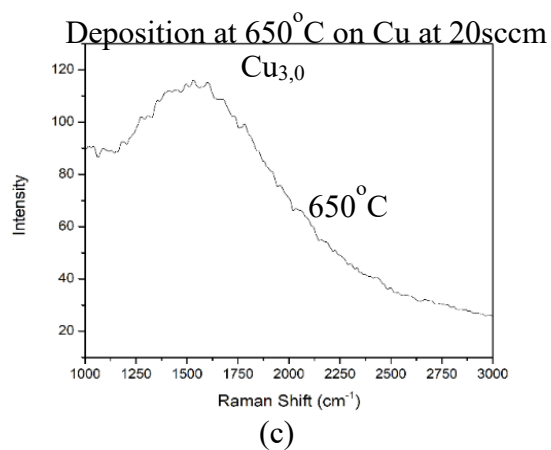
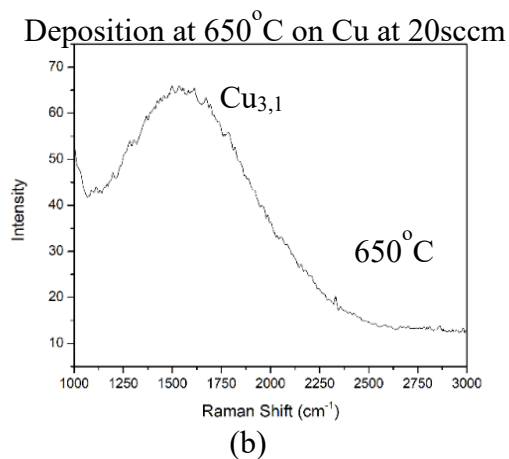
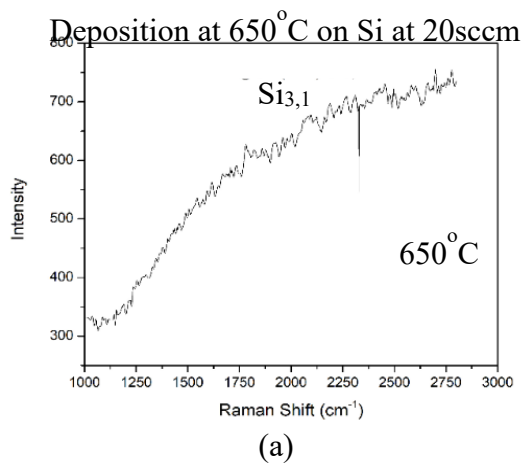
We further increased the temperature of the resistive heater to 850°C at an increment of 50°C, it was observed we had a CBM at both laser incident and non-incident regions and the D, G, and 2D peaks were around the same ballpark of Raman shifts reported above.

Table 3.3 Constant CH₄ flow rate at 20sccm and varied temperature

Sample ID	Process parameters				
	Temp (°C)	Laser pulse frequency (Hz)	CH ₄ flow rate (sccm)	Deposition time (min)	
Cu _{3,0}	650	10	20	5	
Si _{3,1}	Cu _{3,1}	650	10	20	5
Cu _{5,0}	700	10	20	5	
Si _{5,1}	Cu _{5,1}	700	10	20	5
Cu _{7,0}	750	10	20	5	
Si _{7,1}	Cu _{7,1}	750	10	20	5
Cu _{9,0}	800	10	20	5	
Si _{9,1}	Cu _{9,1}	800	10	20	5
Cu _{11,0}	850	10	20	5	
Si _{11,1}	Cu _{11,1}	850	10	20	5

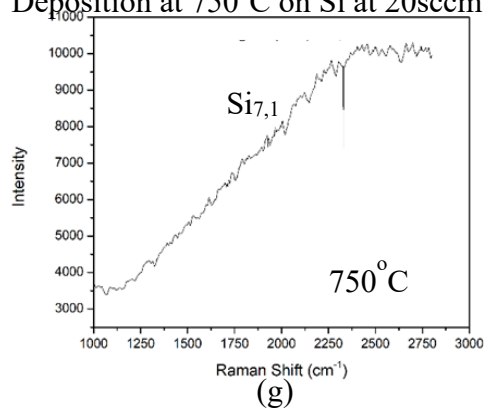
This means at 20sccm, we generated sufficient mass diffusion and flux from the gas phase and the substrate surface to initiate the reaction. Also, the photons from the pulsed laser effectively raised the local temperature of the bombarded region and heat was sufficiently conducted to the non-laser bombarded regions to promote the growth of our CBM by breaking the carbon-hydrogen bonds at its dehydrogenation energy to produce sp² hybridized carbon.

It was observed that our CBMs were highly defective because of the prominence of the intensity of the D peak when compared with high quality graphene in Figure 3.1 (c).

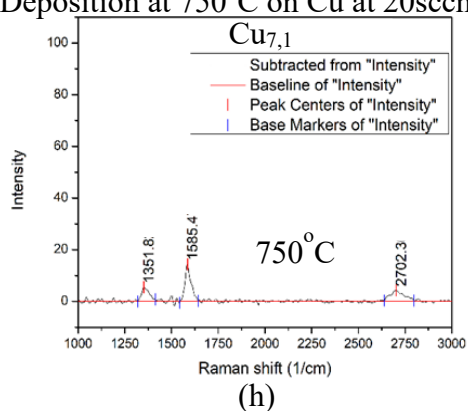


Figures 3.3 (a-f) Raman spectra at constant CH₄ flow rate at 20sccm and varied temperature

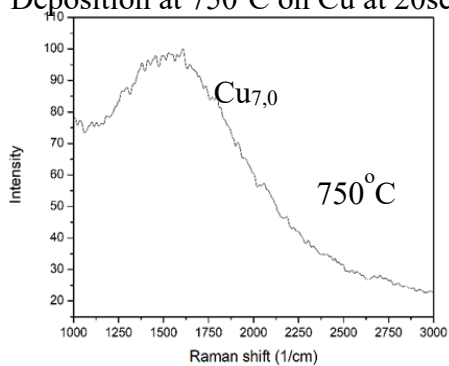
Deposition at 750°C on Si at 20sccm



Deposition at 750°C on Cu at 20sccm

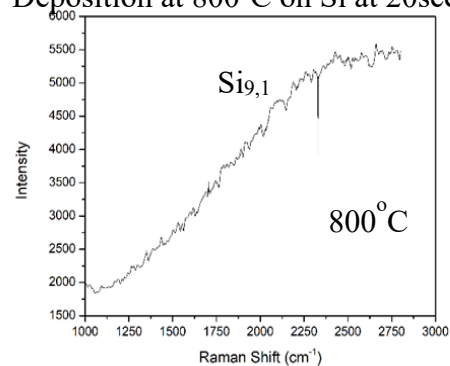


Deposition at 750°C on Cu at 20sccm



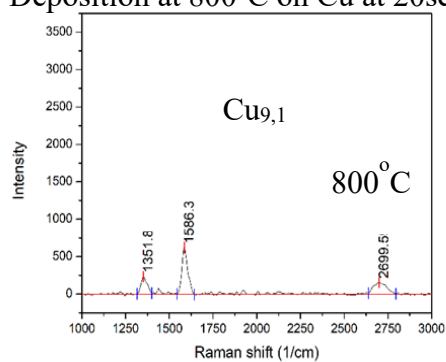
(i)

Deposition at 800°C on Si at 20sccm



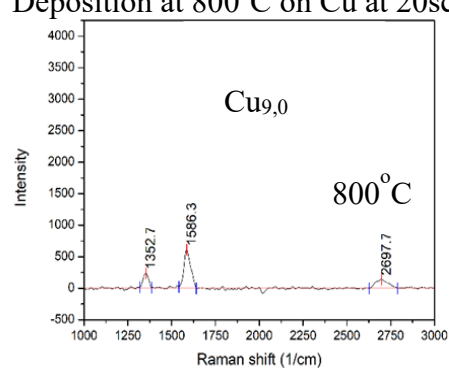
(j)

Deposition at 800°C on Cu at 20sccm



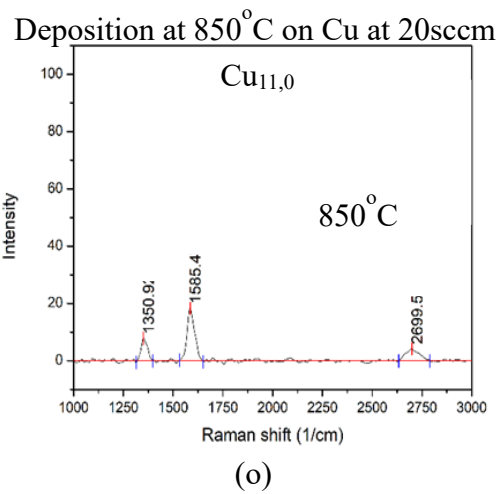
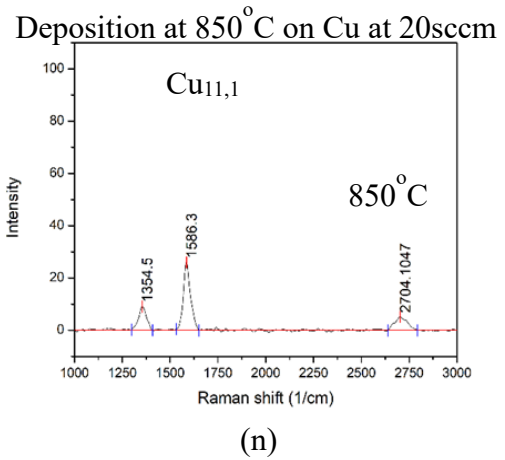
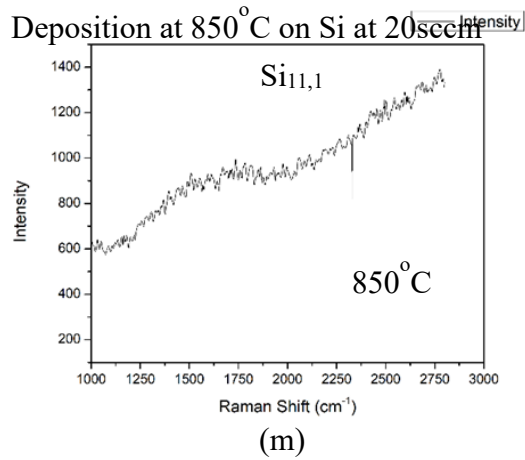
(k)

Deposition at 800°C on Cu at 20sccm



(l)

Figures 3.3 cont'd (g-l) Raman spectra at constant CH₄ flow rate at 20sccm and varied temperature



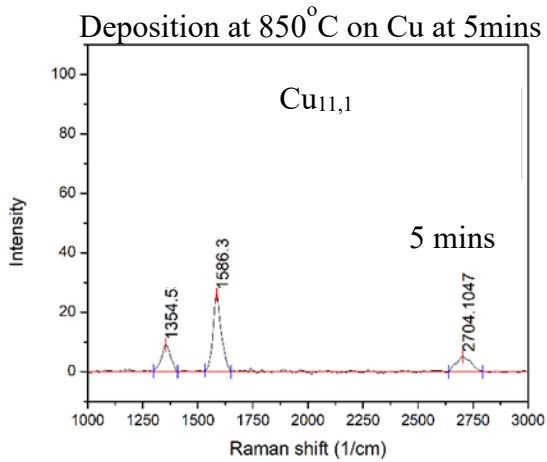
Figures 3.3 cont'd (m-o) Raman spectra at constant CH₄ flow rate at 20sccm and varied temperature

3.3 Variation of time

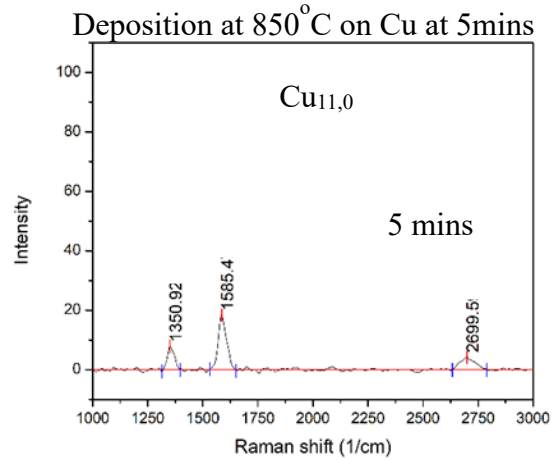
Here we vary the time and kept every other parameter constant as shown in Table 3.4 below and seen in Figures 3.4 (a-f).

Table 3.4 Constant CH₄ flow rate at 20sccm, temperature and varied time

Sample ID	Process parameters			
	Temp (°C)	Laser pulse	CH ₄ flow rate	Deposition
		frequency (Hz)	(sccm)	time (min)
Cu _{11,0}	850	10	20	5
Cu _{11,1}	850	10	20	5
Cu _{12,0}	850	10	20	3
Cu _{12,1}	850	10	20	3
Cu _{13,0}	850	10	20	1
Cu _{13,1}	850	10	20	1

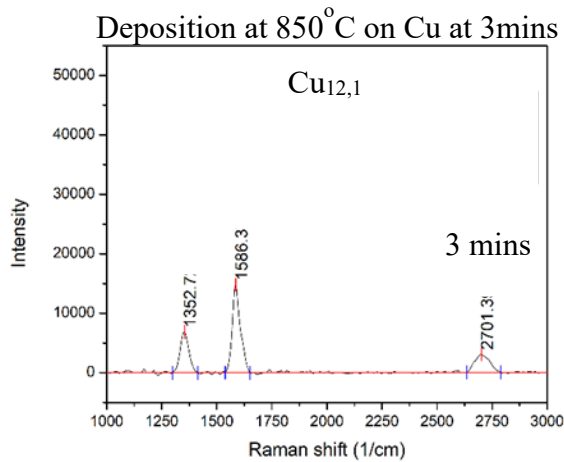


(a)

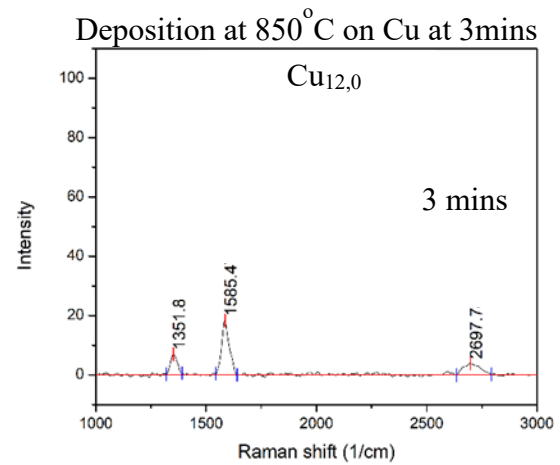


(b)

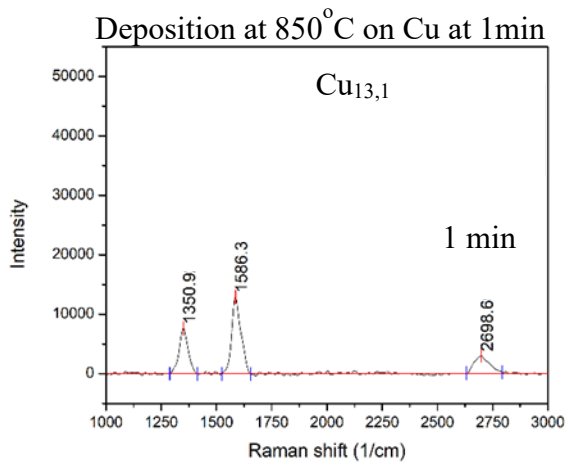
Figures 3.4 (a-b) Raman spectra at constant CH₄ flow rate of 20sccm, temperature and varied time



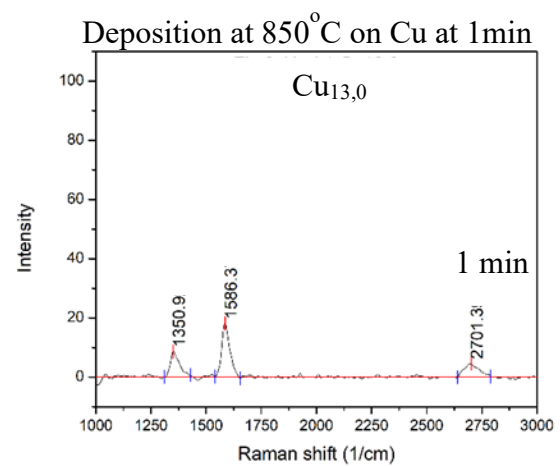
(c)



(d)



(e)



(f)

Figures 3.4 cont'd (c-f) Raman spectra at constant CH_4 flow rate of 20sccm, temperature and varied time

We decided to reduce the deposition time of our CBM as we suspected to be multi-layer graphene in a bid to sharpen our 2D peak (graphene is known to possess sharp 2D peaks as seen in Figure 3.1 (c)) by reducing the number of layers. The deposition time was reduced from 5 to 3 and then to 1 minute, but there was no significant improvement of the 2D peak, this made us conclude that we might not have graphene but rather a graphene-like material.

This prompted us to do some extensive literature study on why we had no improvement of our 2D peak. It was observed that what we deposited was pyrolytic carbon (PyC)- it is produced by heating a hydrocarbon (in this case CH₄) nearly to its thermal decomposition temperature (1000°C-1200°C), breaking its bonds to form carbon free radicals, subsequent covalent bonding and letting the graphite to crystalize in the absence of oxygen (pyrolysis)³⁸.

Pyrolytic carbon (PyC) films comprise of randomly oriented and intertwined graphene flakes, with the average size of a few nanometers³⁹ causing it to exhibit anisotropic properties and some amount of surface roughness. This surface roughness does not change considerably with film thickness,⁴⁰ and it is also responsible for quenching the 2D signal as seen in samples Cu_{11,1}, Cu_{12,1}, and Cu_{13,1} no matter how we change the deposition time.

PyC has a density of 2200 kg/m³, flexural strength (AB) 89.6MPa, compressive strength (AB) 103.4MPa, compressive strength (C) 172.4MPa, shear strength (AB) 6.9MPa, thermal conductivities of 400W/(mK) and 3.5W/(mK) along AB and C planes respectively⁴¹.

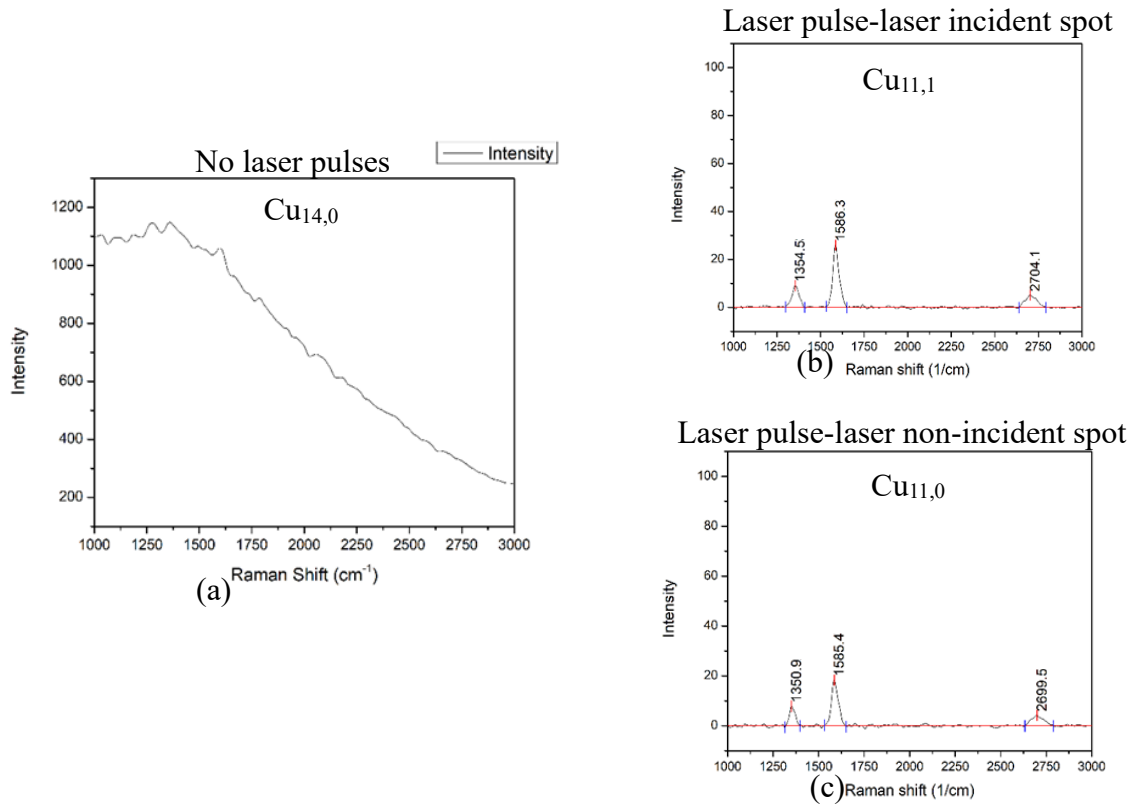
It has been reported that it is a chemically stable material and has remarkably high absorption loss of up to 50% of incident power, making PyC films a suitable candidate for electromagnetic interference shielding in space and airspace communication systems, and portable electronic devices⁴².

3.4 Effect of laser energy on PyC deposition

Here we compare 2 depositions, one grown by purely thermal CVD and the other laser-assisted CVD as shown in Table 3.5 and Figures 3.5 below.

Table 3.5 Effect of laser energy on PyC deposition

Sample ID	Process parameters				
	Temp (°C)	Laser pulse frequency (Hz)	CH ₄ flow rate (sccm)	Deposition time (min)	
Cu _{11,0}	850	10	20	5	
Si _{11,1}	Cu _{11,1}	850	10	20	5
	Cu _{14,0}	850	0	20	5



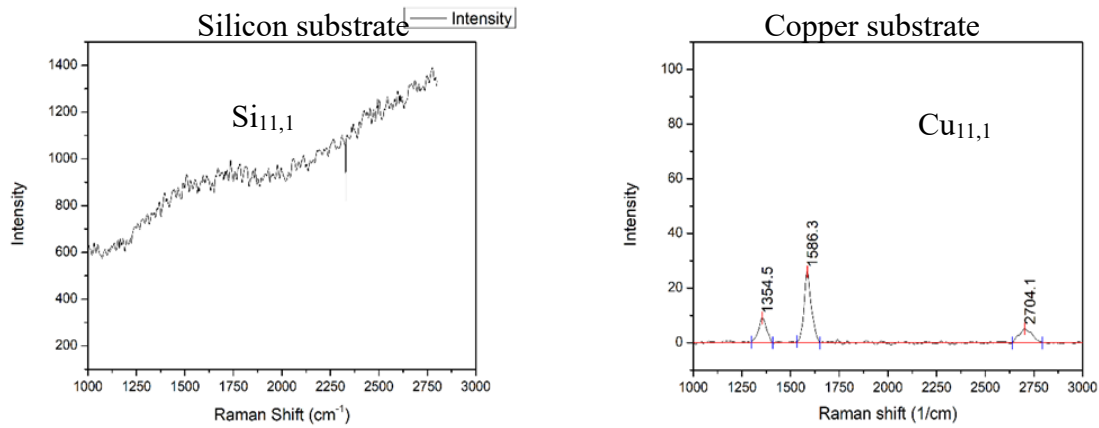
Figures 3.5 (a-c) Raman data plots showing effect of pulsed laser on PyC deposition

Here, we observe the impact of pulsed laser on the growth of PyC, we consider samples Cu₁₁ and Cu₁₄. All D, G and 2D peaks were observed in the laser and non-laser bombarded regions of sample Cu₁₁, this means the laser shots create a local laser bombardment region and serves as a complementary source of energy, this raises the local temperature of the laser spot providing the additional energy needed to initiate the reaction and have the substrate conduct heat to non-laser incident areas, increasing the deposition area. For the Cu₁₄ sample, the thermal energy supplied exclusively from the resistive heater was insufficient to initiate PyC deposition.

3.5 Effect of substrate on PyC deposition

We compare how both silicon and copper substrates fared in deposition of PyC at 850°C and the process parameters set to 10Hz, CH₄ flow rate of 20sccm and deposition time of 5 mins.

Although our Raman spectra for the silicon substrate did not produce any distinguishable peak that connotes the presence of PyC, but the bump-like pattern of our graph shows the presence of amorphous carbon. In contrast, the copper substrate shows crystalline sp² hybridized in form of PyC evident by the D, G and 2D peaks in Raman spectrum. What this tells us is that the copper substrate serves as a catalyst to aid the deposition of pyrolytic carbon by aiding the surface solubility of carbon on copper. The Raman plots are shown in Figures 3.6 below.



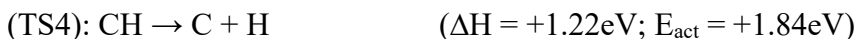
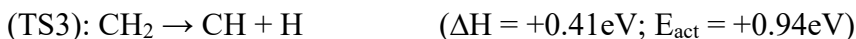
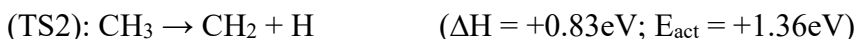
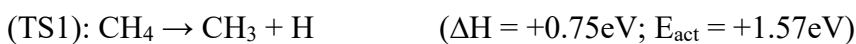
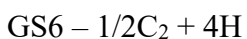
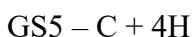
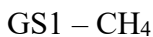
Figures 3.6 Raman data plots showing effect of pulsed laser on PyC deposition

3.6 Reaction mechanism for PyC deposition

We analyze the reaction pathways for CH₄ decomposition and dehydrogenation over the copper substrate surface by taking a cue from Gajewski, Grzegorz & Pao, Chun-Wei. (2011)⁴⁷. Their computations were performed with the Vienna ab initio simulation package (VASP) using projector-augmented wave potentials and the PerdewBurke-Ernzerhof (PBE) functional to investigate the minimum energy pathways (MEP) of successive dehydrogenation reactions of CH₄. The reaction mechanisms that took place on the surface of the copper substrate are as follows:

1. Physisorption of CH₄
2. Adsorptions of CH₃ and CH₃ + H
3. Adsorptions of CH₂ and CH₂ + H
4. Adsorptions of CH and CH + H
5. Adsorptions of C and C + H
6. Adsorption of H
7. Adsorption of C₂

Since the dehydrogenation process is a multi-step process with a series of intermediates, therefore we have multiple ground and transition states. There are 6 ground states (GS) and 4 transitional states (TS) for this reaction which is shown below:



The activation barriers for CH_4 decomposition in the gas phase is much higher than that of the surface of the copper substrate. All four reactions for the transitional states are endothermic. As a matter of fact, all the reactions are endothermic except for the formation of carbon dimer C_2 , the most important step for the graphene growth on the copper substrate. The overall reaction is given as,



The energy profile for the complete dehydrogenation process is shown in Figure 3.7 below.

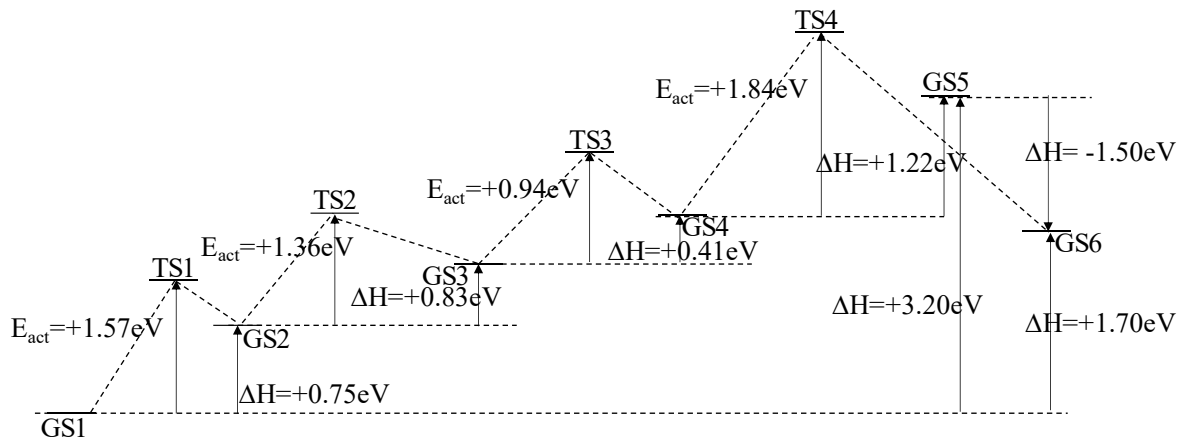


Figure 3.7 Energy profile for the complete dehydrogenation of CH_4 ⁴⁷

3.7 Quantitative analysis of results

Next, we quantitatively analyze our results. The number of layers can easily be calculated by either taking the ratio of D and G or 2D and G peak intensities⁴⁶, the ratio of the areas of the respective peaks can be used to compute the number of layers as well. The Table 3.7 below shows the approximate ratio of intensities by number of graphene layers.

The Table 3.8 below shows the peak positions, intensity, and the number of layers obtained from each deposition we were able to get Raman signal for. From the Table 3.8 below, we can conclude after taking ratios of the intensities that all the samples we grew have many flakes/layers of graphene. The same information can be obtained if we take the ratio of the areas instead for each respective peak. Sample Cu_{15} is the commercial grade graphene we purchased and used as the gold standard for our deposition. Here we can see that it is a single layer graphene with zero defect. It can be seen from the D peak that sample $\text{Cu}_{13,1}$ has the highest defect concentration, the defect data looks rather inconclusive, and more research needs to be done on this, same goes for the carbon concentration shown from the G peak.

Table 3.7 Ratio of peak intensities and number of layers

Number of graphene layers	Approximate peak intensities	
Single layer	$\frac{I_D}{I_G} = 0$	$\frac{I_{2D}}{I_G} = 2$
Double layer	$\frac{I_D}{I_G} = 0.05$	$\frac{I_{2D}}{I_G} = 1$
Few layer	$\frac{I_D}{I_G} = 0.1$	$\frac{I_{2D}}{I_G} = 0.8$
Multi-layer	$\frac{I_D}{I_G} = 0.18$	$\frac{I_{2D}}{I_G} = 0.5$

In a nutshell, at 20sccm flow rate of CH₄, sufficient mass diffusion and flux from the gas phase and the substrate surface was generated to initiate the reaction. In addition, photons from the pulsed laser at an energy density of 0.116J/cm² per pulse and 10Hz was sufficient to cause deposition of amorphous and crystalline carbon at a minimum of 750°C on both silicon and copper substrates, respectively. The photons from the pulsed laser effectively raised the local temperature of the bombarded region, and heat was sufficiently conducted to the non-laser bombarded regions to promote the growth of PyC by breaking the carbon-hydrogen bonds at its dehydrogenation energy to produce sp² hybridized carbon. Copper has a catalytic influence in PyC deposition because it promotes the surface solubility of carbon. PyC is defect ridden unlike high quality graphene because of the intertwined nature of its graphene flakes that causes surface roughness and quenching of the 2D peak.

Table 3.8 Peak positions, intensities, and number of layers

ID	Peak position			Peak intensity			$\frac{I_{2D}}{I_G}$	Peak area			$\frac{A_{2D}}{A_G}$
	D	G	2D	D	G	2D		D	G	2D	
Cu _{7,1}	1351	1585	2702	5.5	14.3	4.2	0.3	267.1	548.4	377.4	0.7
Cu _{9,0}	1352	1586	2697	237.3	612.9	142.3	0.2	8828.0	27855.0	11766.2	0.4
Cu _{9,1}	1351	1586	2699	234.2	621.5	155.2	0.3	9723.4	24434.8	13616.0	0.6
Cu _{11,0}	1350	1585	2699	7.8	18.3	4.2	0.2	294.9	822.5	330.7	0.4
Cu _{11,1}	1354	1586	2704	9.1	26.0	5.1	0.2	451.4	1157.6	401.9	0.4
Cu _{12,0}	1351	1585	2697	6.9	18.3	3.8	0.2	263.6	752.8	350.1	0.5
Cu _{12,1}	1352	1586	2701	6858	14769	3103	0.2	320096.0	644120.2	249714.2	0.4
Cu _{13,0}	1350	1586	2701	8.6	18.1	4.5	0.3	427.3	792.3	365.5	0.5
Cu _{13,1}	1350	1586	2698	7607	12899	3008	0.2	366476	633137	250835	0.4
Cu ₁₅	0	1589	2677	0	140.6	375.4	2.7	0	5129.9	15718.5	3.1

CONCLUSIONS AND FUTURE WORKS

The following research findings are given below:

1. With an energy density of $0.116\text{J}/\text{cm}^2$ per pulse, the minimum mass flow rate of CH_4 is required to initiate a deposition is 20sccm . This value is not a universal constant for all depositions as this value differs from those of other publications⁴³⁻⁴⁵ because the dimension of the deposition chamber, pressure, and the distance between the gas inlet and the substrate, mass diffusion and flux from the gas phase and the substrate surface play a significant role on how fast the carbon source gas populate the chamber and how far the gas needs to diffuse to get to the reaction zone.
2. The minimum temperature required to get pyrolytic carbon signals in Raman spectroscopy i.e., the D, G and 2D peaks is 750°C with a laser energy density of $0.116\text{J}/\text{cm}^2$ per pulse. For this to happen at 750°C and higher temperature, a laser pulse frequency of 10Hz is required to effectively dehydrogenate the CH_4 gas and create free radicals for deposition to occur.
3. The presence of laser shots creates a local laser bombardment region which raises the local temperature of the laser spot providing the additional thermal energy needed to initiate the reaction.
4. Copper foil is a more suitable substrate to grow pyrolytic carbon than silicon dioxide wafer using our experimental setup because copper aids the surface solubility of carbon.
5. From Raman data, we can safely conclude that pyrolytic carbon does share similar characteristics with graphene because of the coinciding Raman shifts of the D, G and 2D peaks at 1350cm^{-1} , 1600cm^{-1} , and 2700cm^{-1} respectively because pyrolytic carbon (PyC)

is simply randomly oriented and intertwined graphene flakes produced by heating a hydrocarbon nearly to its thermal decomposition temperature breaking its bonds to form carbon free radicals, subsequent covalent bonding and letting the graphite to crystalize in the absence of oxygen (pyrolysis).

6. Pyrolytic carbon is relatively more defect-ridden than high quality graphene because of the intertwined nature of its constituent graphene flakes. Despite having graphene as its fundamental building block, the intertwining of the graphene flakes induces some surface roughness which does not change considerably with film thickness, and it is also responsible for quenching the 2D peak on the Raman spectra no matter how we change the deposition time as seen in samples Cu_{11,1}, Cu_{12,1} and Cu_{13,1}.

We have seen the impact of laser irradiation on the deposition of pyrolytic carbon using optimal deposition parameters on copper substrate. In future, we intend to repeat this experiment using inductive heating as our primary source of thermal energy, observe if the presence of laser plays a similar role to the resistive heating technique, transfer the pyrolytic carbon on a silicon dioxide substrate and then measure its transport properties.

REFERENCES

- (1) Backes, C.; Abdelkader, A.; Alonso, C.; Andrieux-Ledier, A.; Arenal, R.; Azpeitia, J. *Production and Processing of Graphene and Related Materials*. *2D Materials* **2020**, 7(2), 022001.
- (2) Wang, J.; Ren, Z.; Hou, Y.; Yan, X.; Liu, P.; Zhang, H. *A Review of Graphene Synthesis at Low Temperatures by CVD Methods*. *New Carbon Materials* **2020**, 35(3), 193-208.
- (3) Kim, B.; Nasir, T.; & Choi, J. *Direct Growth of Graphene at Low Temperature for Future Device Applications*. *Journal of The Korean Ceramic Society* **2018**, 55(3), 203-223.
- (4) Fuente, J. *Graphene - What Is It?* <https://www.graphenea.com/pages/graphene#.x4cnk2hkjiu> (accessed 10/14/2020).
- (5) Staff, S. *What Is Graphene?* *Sciencealert*. <https://www.sciencealert.com/graphene> (accessed 10/14/2020).
- (6) Wang, C.; Vinodgopal, K.; Dai, G. *Large-Area Synthesis and Growth Mechanism of Graphene by Chemical Vapor Deposition*. *Chemical Vapor Deposition for Nanotechnology* **2019**, 5.
- (7) Karim, M.; Hayami, S. *Chemical, Thermal, and Light-Driven Reduction of Graphene Oxide: Approach to Obtain Graphene and Its Functional Hybrids*. *Graphene Materials - Advanced Applications* **2017**, 5.
- (8) Brownson, D.; Banks, C. *The Handbook of Graphene Electrochemistry* **2014**, 12.
- (9) Skákalová, V.; Kaiser, A. *Graphene: Properties, Preparation, Characterisation and Devices* **2014**, 4-21.
- (10) Yazdi, G.; Iakimov, T.; Yakimova, R. *Epitaxial Graphene on Sic: A Review of Growth and Characterization*. *Crystals* **2016**, 6(5), 53.
- (11) Yang, X.; Zhang, G.; Prakash, J.; Chen, Z.; Gauthier, M.; Sun, S. *Chemical Vapour Deposition of Graphene: Layer Control, The Transfer Process, Characterisation, and Related Applications*. *International Reviews in Physical Chemistry* **2019**, 38(2), 149-199.
- (12) Bolotin, K.; Sikes, K.; Jiang, Z.; Klima, M.; Fudenberg, G.; Hone, J. *Ultrahigh Electron Mobility in Suspended Graphene*. *Solid State Communications* **2008**, 146(9-10), 351-355.

- (13) *Graphene Synthesis, Properties, and Applications* <https://www.cheaptubes.com/graphene-synthesis-properties-and-applications/> (accessed 10/16/2020).
- (14) *Understanding Graphene* <https://www.nanowerk.com/infographics/graphene-infographic-large.jpg> (accessed 10/16/2020).
- (15) Mccallion, C.; Burthem, J.; Rees-Unwin, K.; Golovanov, A.; Pluen, A. *Graphene in Therapeutics Delivery: Problems, Solutions, and Future Opportunities. European Journal of Pharmaceutics and Biopharmaceutics* **2016**, 104, 235-250.
- (16) Sameh T. *Data Science + Graphene Synthesis* <https://nanohub.org/resources/33340> (accessed 10/17/2020).
- (17) Malandrino, G. *Chemical Vapour Deposition. Precursors, Processes and Applications*. Edited by Anthony C. J.; Michael L. H. *Angewandte Chemie International Edition* **2009**, 48(41), 7478-7479.
- (18) *Chemical Vapor Deposition* http://users.wfu.edu/ucerkb/nan242/l09-cvd_a.pdf (accessed 10/17/2020).
- (19) Xu, Y., & Yan, X. *Chemical Vapour Deposition. Engineering Materials and Processes* **2010**, 146-161.
- (20) Grove, A. *Physics and Technology of Semiconductor Devices* **1967**, 10-11.
- (21) *Chemical Vapor Deposition (cont.)* http://users.wfu.edu/ucerkb/nan242/l10-cvd_b.pdf (accessed 10/17/2020).
- (22) Sivaram, S. *Chemical Vapor Deposition: Thermal and Plasma Deposition of Electronic Materials* **1995**, 95.
- (23) *Fluid Measurement and Control* https://www.horiba.com/en_en/fluid-measurement-and-control/ (accessed 03/06/2021).
- (24) *MKS Four Channel Readout* <http://uhv.cheme.cmu.edu/manuals/mks.fourchannelreadout.pdf.pdf> (accessed 03/16/2021).
- (25) Naik, P. *Vacuum Science, Technology and Applications* **2018**, 109.
- (26) Bello, I. *Vacuum and Ultravacuum: Physics and Technology* **2017**, 490-494.
- (27) Bannwarth, H. *Liquid Ring Vacuum Pumps, Compressors, and Systems: Conventional and Hermetic Design* **2005**, 117.

- (28) Chambers, A. *Modern Vacuum Physics* **2004**, 143-145.
- (29) Powell, R. *Physics of Solid-State Laser Materials* **1998**, 294-295.
- (30) *Diode Laser Pumped Nd: YAG Laser*
https://www.tau.ac.il/~lab3/72_laser_res/yag_manual.pdf (accessed 03/20/2021).
- (31) Shaik, A. *Nd:YAG Laser - Definition, Construction and Working* <https://www.physics-and-radio-electronics.com/physics/laser/ndyaglaser.html> (accessed 03/20/2021).
- (32) *What Is Nd:YAG Laser?- Definition, Construction, Working and Applications Of Nd:YAG Laser - Circuit Globe* <https://circuitglobe.com/ndyag-laser.html> (accessed 03/20/2021).
- (33) *The Joule Heating Effect* <https://www.comsol.com/multiphysics/the-joule-heating-effect?parent=electromagnetics-072-92> (accessed 03/21/2021).
- (34) *Electric and Induction Heating* http://www.idc-online.com/technical_references/pdfs/electrical_engineering/electric_and_induction_heating.pdf (accessed 03/21/2021).
- (35) Edwards, H. *Modern Raman Spectroscopy—A Practical Approach*. Ewen Smith and Geoffrey Dent. John Wiley and Sons Ltd, Chichester, 2005. Pp. 210. *Journal of Raman Spectroscopy* **2005**, 36(8), 835-835.
- (36) Bumbrah, G.; Sharma, R. *Raman Spectroscopy – Basic Principle, Instrumentation and Selected Applications for the Characterization of Drugs of Abuse*. *Egyptian Journal of Forensic Sciences* **2016**, 6(3), 209-215.
- (37) *Principles of Raman Spectroscopy. What Is Raman Spectroscopy?* <https://www.jasco-global.com/principle/1-what-is-raman-spectroscopy/> (accessed 03/23/2021).
- (38) *Pyrolytic Carbon* https://en.wikipedia.org/wiki/pyrolytic_carbon (accessed 03/28/2021).
- (39) Batrakov, K.; Kuzhir, P.; Maksimenko, S.; Paddubskaya, A.; Voronovich, S.; Kaplas, T.; Svirko, Y. *Enhanced Microwave Shielding Effectiveness of Ultrathin Pyrolytic Carbon Films*. *Applied Physics Letters* **2013**, 103(7), 073117.
- (40) Dovbeshko, G.; Romanyuk, V.; Pidgirnyi, D.; Cherepanov, V.; Andreev, E.; Levin, V. *Optical Properties of Pyrolytic Carbon Films Versus Graphite and Graphene*. *Nanoscale Research Letters* **2015**, 10(1), 234.
- (41) Bajpai, V.; Singh, R. *Orthogonal Micro-Grooving of Anisotropic Pyrolytic Carbon*. *Materials and Manufacturing Processes* **2011**, 26(12), 1481-1493.

(42) Voronovich, S.; Paddubskaya, A.; Batrakov, K.; Kuzhir, P.; Maksimenko, S.; Kaplas, T.; Svirko, Y. *Electromagnetic Properties of Graphene-Like Films in Ka-Band*. *Applied Sciences* **2014**, *4*(2), 255-264.

(43) Jiang, J.; Lin, Z.; Ye, X.; Zhong, M.; Huang, T.; Zhu, H. *Graphene Synthesis by Laser-Assisted Chemical Vapor Deposition on Ni Plate, and the Effect of Process Parameters on Uniform Graphene Growth*. *Thin Solid Films* **2014**, *556*, 206-210.

(44) Zhang, C.; Zhang, J.; Lin, K.; Huang, Y. *Laser-Assisted Chemical Vapor Deposition Setup for Fast Synthesis of Graphene Patterns*. *Review of Scientific Instruments* **2017**, *88*(5), 053907.

(45) Um, J.; Kim, S.; Lee, B.; Park, J.; Jeong, S. *Direct Writing of Graphite Thin Film by Laser-Assisted Chemical Vapor Deposition*. *Carbon* **2020**, *169*, 163-171.

(46) *Graphene Number of Layers Calculator From ID/IG and I2D/IG Ratio via Raman Spectroscopy* <https://www.instanano.com/2017/03/raman-characterization-graphene.html> (accessed 04/17/2021).

(47) Gajewski, G.; Pao, C. *Ab Initio Calculations of the Reaction Pathways For Methane Decomposition Over The Cu (111) Surface*. *The Journal of Chemical Physics* **2011**, *135*(6), 064707.